Mechanistic Study of Carbazole and Triphenylamine Dimerization and Pyrrolidine Dehydrogenation Using Mass Spectrometry

A thesis presented to

the faculty of

the College of Arts and Sciences of Ohio University

In partial fulfillment

of the requirements for the degree

Master of Science

Brian E. Hivick

May 2019

This thesis titled

Mechanistic Study of Carbazole and Triphenylamine Dimerization and Pyrrolidine Dehydrogenation Using Mass Spectrometry

by

BRIAN E. HIVICK

has been approved for

the Department of Chemistry and Biochemistry

and the College of Arts and Sciences by

Hao Chen

Professor of Chemistry and Biochemistry

Joseph Shields

Interim Dean, College of Arts and Sciences

ABSTRACT

HIVICK, BRIAN E., M.S., May 2019, Chemistry

Mechanistic Study of Carbazole and Triphenylamine Dimerization and Pyrrolidine Dehydrogenation Using Mass Spectrometry

Director of Thesis: Hao Chen

Mass spectrometry is one of the most powerful techniques used in analytical chemistry today. It has been utilized in a wide variety of fields, from synthesis to pharmaceuticals to analyzing medicinal samples. One of its greatest strengths is its ability to be combined with other techniques to further improve the collected data. In this work, the ability to couple mass spectrometry with electrochemistry in the dimerization of two aromatic amines, carbazole and triphenylamine, is explored, and insight into the underlying dimerization mechanism is achieved. In addition, photochemistry is also coupled with mass spectrometry, and the potential dehydrogenation of pyrrolidine is explored.

DEDICATION

I dedicate this work to my parents and siblings, who have done so much for me throughout my life and have unequivocally supported me in all of my decisions.

ACKNOWLEDGMENTS

I would like to acknowledge my advisor, Dr. Hao Chen, for all of his support and faith in me throughout my research, even when I did not have any faith.

I would also like to acknowledge my thesis committee members, Dr. Peter de B. Harrington and Dr. Travis A. White, for their feedback not only on my thesis, but throughout my graduate career.

I would like to acknowledge my group members Dr. Chengyuan Liu, Chang Xu, Yuexiang Zhang, Pengyi Zhao, Yue Tang, and Qi Wang for their help and support throughout my work.

I would like to acknowledge the faculty and staff of the Department of Chemistry and Biochemistry for always being willing and ready to help at a moment's notice. In particular, I would like to acknowledge Jackie Bennett-Hanning, Paul Schmittauer, Bascom French, Aaron Dillon, Dr. Rebecca Barlag, and Dr. Andrew Tangonan for directly supporting this work in a variety of ways.

TABLE OF CONTENTS

Page

LIST OF SCHEMES

Page

LIST OF FIGURES

Page

CHAPTER 1: INTRODUCTION

1.1 Mass Spectrometry

Mass spectrometry (MS) is among the most powerful and widely used analytical techniques. Using MS, it is possible to analyze ionized samples based on their mass-to-charge ratio (*m/z*).[1] By determining the charge of the species, it is therefore easy to identify its' mass, which can allow identifying the compound. In addition, tandem mass spectrometry (MS/MS or MS^2) can be performed, wherein a given ion can be isolated with the MS and then fragmented into smaller pieces, which will then be detected. This allows MS to be used as a powerful tool for structural analysis of compounds.[2] Mass spectrometry has been successfully used for all kinds of compounds, from small organic molecules[3], to metallic-based samples[4], to large biological macromolecules such as proteins[5]. Due to its versatility and aptitude for identification, MS has been incorporated in numerous fields, including forensics[6], drug development[7], environmental analysis[8], and compound synthesis[9].

1.2 Mass Spectrometer

Although mass spectrometers can be designed in a variety of ways depending on the purpose they will be used for, there are typically a few common components across mass spectrometers. These include an ionization source, which generates charged ions for analysis; ion optics, which are used to filter and guide the ions that enter the instrument; a mass analyzer, which separates out the different ions based on their mass-to-charge ratio; and a detector, which converts the energy of the ions that reach it into electric signal,

which can they be transferred to a workstation as a spectra[5]. In addition, a vacuum system is typically used with mass spectrometry, and is vital to the operation of the instrument.

1.3 Ionization Methods

There are numerous different methods which have been used for the generation of ions before they enter the instrument. One of the first methods developed was electron ionization (EI), in which compounds are bombarded by high energy electrons, leading the occurrence of ionization.[10] Another early method used was chemical ionization (CI), in which a reagent gas is ionized, which in turn reacts with the analyte of interest to cause the analyte to undergo ionization[11]. However, these early techniques had considerable flaws, including fragmentation of the analyte and the inability to be used for large molecules[5]. Due to these flaws, considerable effort had been expended on the development of new techniques which allow for a more robust method of ionization, such as electrospray ionization (ESI)[12], matrix-assisted laser desorption ionization (MALDI)[13], and atmospheric pressure chemical ionization (APCI)[14].

Electrospray ionization has become one of the most widely used ionization techniques, due to its high sensitivity and reliability, as well as its ability to analyze biomolecules which do not readily ionize using other techniques[12]. Other benefits of electrospray include that it involves ionization of liquid samples, allowing easy interfacing with separation techniques such as liquid chromatography (LC), as well as its low chemical specificity as to what compounds can undergo ionization[13]. The ionization process for ESI can be divided into three distinct steps (Scheme 1-1)[12]. First, charged droplets of sample are generated from the ESI source. This is accomplished by applying a

sufficiently high voltage (between 2.5 and 6.0 kV[12]) to a capillary tube through which the sample solution is being pumped, generating a Taylor cone[13]. These droplets then travel towards the mass analyzer, during which the droplets are dried by either elevated pressure or a nitrogen drying gas, causing the droplet size to decrease. As these droplets carry a charge, the decrease in size causes an increase in the charge density of the droplet[12]. After the droplet size has decreased sufficiently, the Rayleigh limit is reached[14], at which point the ratio of charge to droplet size has grown too large. Under such a circumstance, the ions in the droplet are either directly ejected into the gaseous phase[12] or split into smaller droplets which further undergo similar de-solvation and splitting until dry ions in the gas phase are formed.

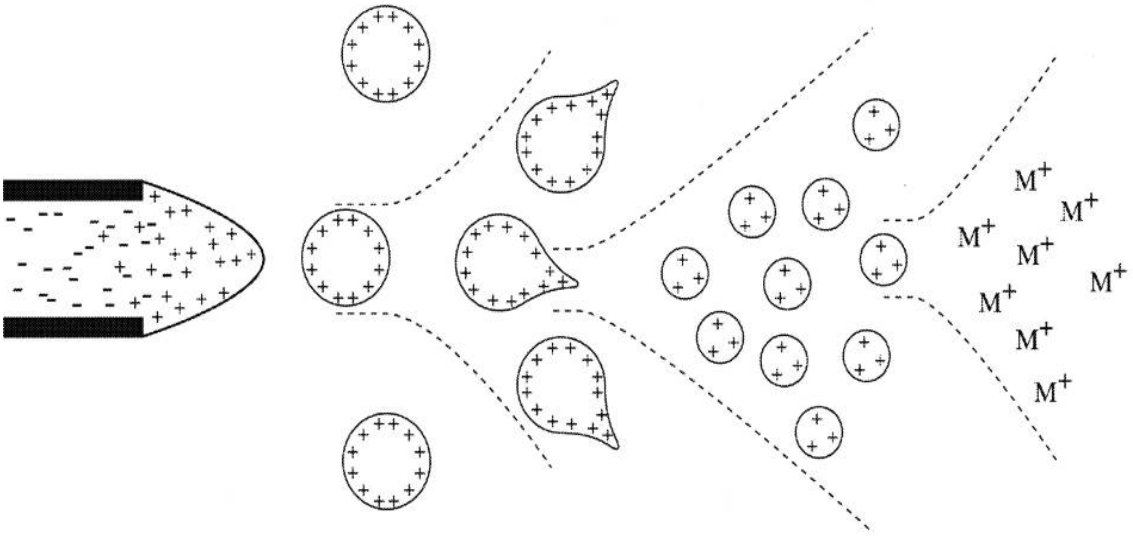

Scheme 1-1: Electrospray ionization process.[13]

Like other methods, ESI is not without its own set of drawbacks. Chiefly among those are the issue of in-source oxidation or in-source reduction taking place due to the use of high potential to begin the ionization process[14], as well as the need to use volatile solvents which will readily evaporate off the charged droplets to produce dry ions. One technique developed to circumvent those issues is desorption electrospray ionization (DESI). In DESI, an electrospray emitter is used to generate charged solvent droplets, following the earlier discussed mechanism, which are directed towards the analyte of interest, instead of the mass spectrometer. As these droplets impact the analyte, the analyte is then dissolved and ionized from the sample, and those ions are then released and travel towards the mass spectrometer inlet (Scheme 1-2). While DESI was first developed with solid samples, it has also been applied to liquids, frozen solutions, and gases that have been adsorbed to a surface.[15]

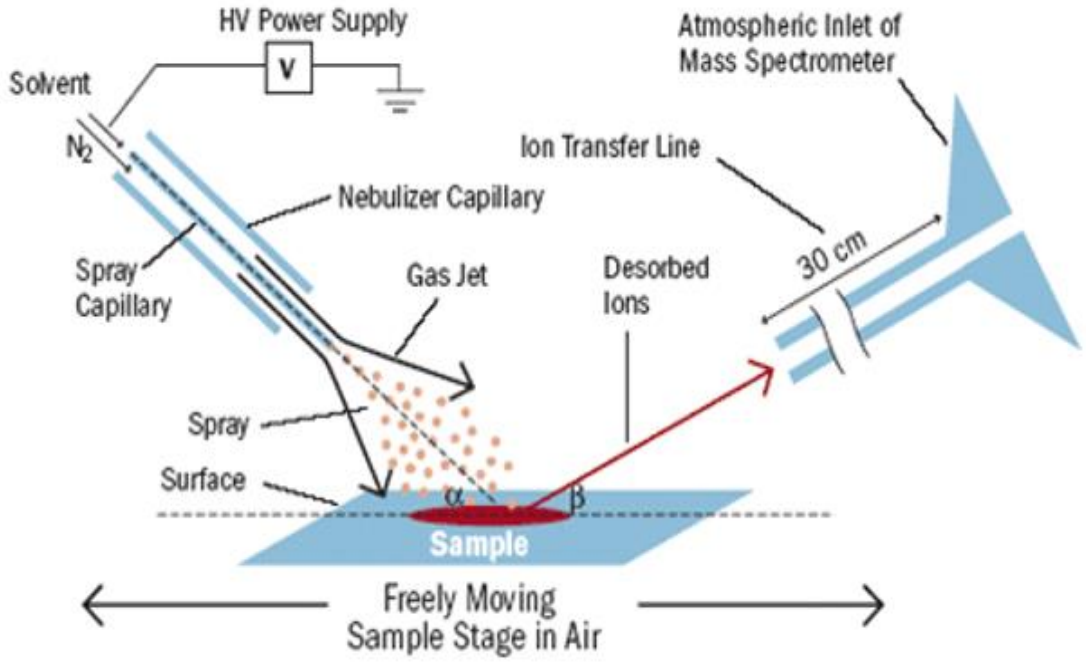

Scheme 1-2: Mechanism of DESI ionization[16]

1.4 Mass Analyzers

The primary function of a mass analyzer is to discriminate between ions based on their *m/z* ratios. There are numerous types of analyzers, some of them can provide very different functions, such as the ability to trap ions of a given *m/z* within the analyzer. Some of the most commonly used types of mass analyzers include quadrupoles, ion traps, time-of-flight (TOF), and Fourier transform-based analyzers such Orbitrap and ion cyclotron resonance (ICR).[17]

One of the commonly used types of mass analyzer is the quadrupole. A quadrupole is made up of four cylindrical rods which are positioned around the path that ions will take (Scheme 1-3). The rods which are directly across from one another carry the same charge, and are connected electrically, with a radio frequency potential applied

to them. A direct current is then also applied over the radio frequency, which causes ions travelling along the rods to oscillate. As ions oscillate, it is possible that they will bump into one of the rods, preventing them from further traveling through the MS. It is then possible to vary the current and radio frequency potential to change which *m/z* of ions will be capable of traveling through the quadrupole, and which will get lost as they bump into the rods.[17] This allows a quadrupole to serve as a filter for only a target *m/z*.[18] Quadrupole mass analyzers are advantageous in their small size, low cost, and high stability, but suffer from limited mass ranges which can be allowed to travel through the quadrupole, as well as poor resolution[17].

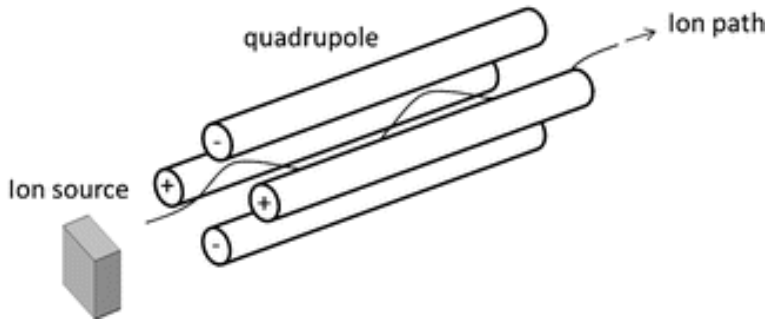

Scheme 1-3: Design of quadrupole mass analyzer[17]

Ion traps are similar in design to quadrupoles, but instead of only allowing target *m/z* ratios to leave the quadrupole, certain *m/z* ratios are instead selected to stay within the ion trap. Non-target ions will be kicked out of the trap, leaving behind only the target species. This allows for accumulation of the target ions, as it is possible to "hold" them within the trap until a sufficient amount is present. The potential is then changed, and the trapped ions are pushed to the detector. Ion traps are often used for MS/MS but have low resolution.[17]

Another of the commonly used mass analyzers is the TOF analyzer (Scheme 1-4). In a TOF analyzer, ions of different *m/z* travel through an electrical potential known as an acceleration grid, where they are imparted with a specific kinetic energy, and begin traveling with a certain velocity based on how much energy is applied and their mass. These ions then travel into a region where no electric field is present, so the ions will maintain their velocity. The detector is positioned at the opposite end of the analyzer, and ions will reach it at different rates depending on the velocity they have after acceleration, which in turn depends on their mass. Then, by measuring the time it takes for ions to reach the detector, it is possible to determine the mass of the ions. The TOF mass analyzers have a high mass range, and can observe very high masses, however they are typically much larger than other analyzers.[17]

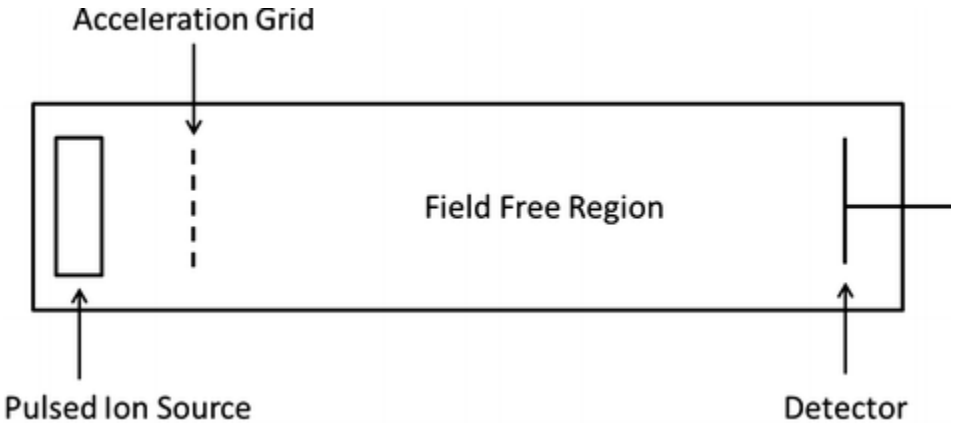

Scheme 1-4: Design of time-of-flight mass analyzer[17]

The Orbitrap is a Fourier-transform based mass analyzer. It consists of three electrodes, two outer electrodes and one central electrode (Scheme 1-5). Ions are injected into the space between the outer and central electrode and are initially tangential to the

central electrode[19]. A potential is then applied between the electrodes, which causes the ions to begin to oscillate around the central electrode. These oscillations can generate imaging current on the outer electrodes which can then be detected, and a Fourier transformation can then be used to generate a mass spectrum.[17] As mass analyzers, Orbitraps have very high resolving power, particularly at high *m/z*. In addition, Orbitraps are relatively small and do not require much maintenance such as the use of expensive liquid helium.[19]

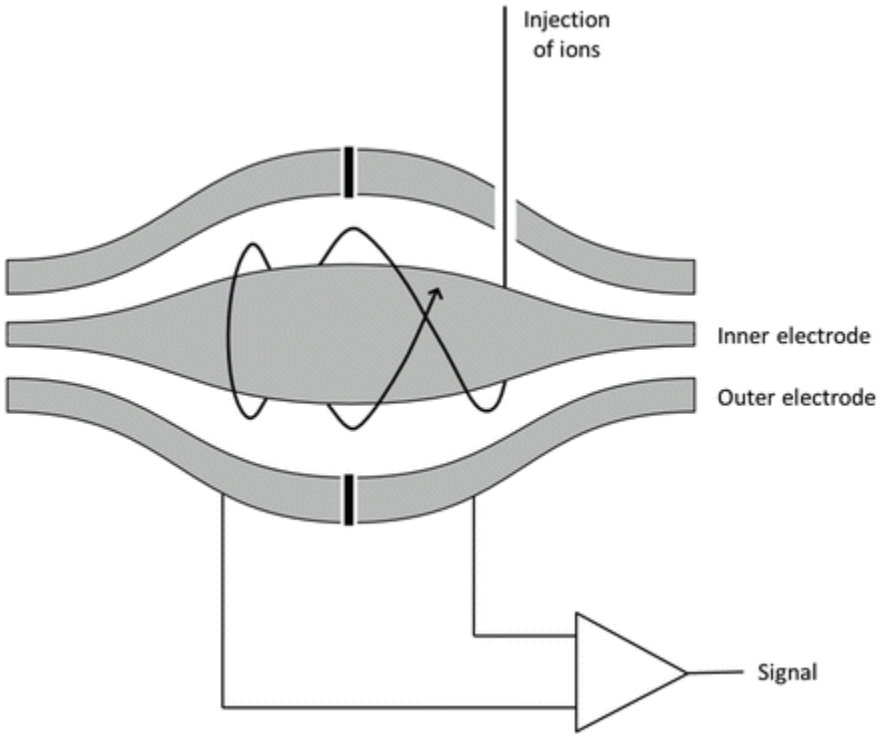

Scheme 1-5: Design of the Orbitrap mass analyzer[17]

1.5 Detectors

Another key portion of the mass spectrometer is the detector. The most commonly used type of detector today is an electron multiplier. Electron multipliers function

similarly to a photon multiplier tube, except it does not have a photon window and instead the first dynode is sensitive to the presence of ions. When ions strike the conversion dynode, secondary electrodes are released, and an electrode cascade takes place, multiplying the signal. The benefits of an electron multiplier as a detector include the high amount of gain from the initial electron, low noise and a large linear dynamic range.[20]

1.6 Coupling Electrochemistry with Mass Spectrometry

Electrochemistry (EC) is a major field of analytical chemistry, with numerous applications independent of MS. Electrochemistry and the techniques under its umbrella have been used to measure redox potentials, examine the reversibility of chemical reactions, and synthesize new materials, *etc*.[21]. Electrochemistry has often been used in tandem with other techniques, such as EC being used detection method for liquid chromatography and biosensors or detecting the products of EC using fluorescence spectroscopy or nuclear magnetic resonance spectroscopy[22]. Recently, significant work has been performed to couple EC with MS, including work in research of numerous fields including drug metabolism[23], environmental metabolites[24], protein structure[25], and oxidative stress[26], among others. Many of these developments are due to advances in ESI, which can readily interface with EC systems. This allows for the online analysis of electrolysis, wherein an EC cell can be toggled between off and on as the sample is injected into the MS, allowing for analysis of the electrolysis process. There are a few concerns which must be addressed when coupling EC with ESI-MS, however. One drawback is that a relatively high potential is necessary for the ionization process, which

needs to be separated from the potential used with the EC cell[22]. One of the benefits of DESI is that this is easy to accomplish, as the analyte is not directly applied with a high voltage, but rather what is impacted by ionized solvent droplets. In addition, many common electrolytes used for EC can impact the resulting mass spectrum, so electrolyte of suitable volatility and concentration must be used[22].

1.7 Coupling Photochemistry with Mass Spectrometry

Photochemistry is also a big area with a wide range of applications, from the synthesis of polymers and other materials[27], to developing photocells to harness energy[28]. When compared to other techniques, photochemistry has numerous benefits, including the ability to drive otherwise difficult reactions with the simple addition of the appropriate light, ease of temporal control due to the ability to simply switch the light on and off, and spatial control provided by controlling where the light is and is not able to sign, whether by adjusting the shape of the light or using masks to protect certain locations from light[29]. Like electrochemistry, photochemistry is an attractive option to couple with MS. Work has been performed to examine the effects of online photochemical reactions, such as those of tetrahydroquinolines[30], zinc phthalocyanine[31], as well as using photochemical tags for analysis fatty acids[32].

CHAPTER 2. STUDY OF CARBAZOLE DIMERIZATION MECHANISM USING EC/MS

2.1 Introduction to Carbazole

Carbazole (CBZ) and triphenylamine (TPA) are two common aromatic amines often used in organic synthesis. Carbazole (Scheme 2-1) and its derivatives can exhibit many useful features, such as being used as photoconductors and the ability to transfer charges. Carbazole first gained interest due to its photoconductivity in the 1950s, with the development of poly(*N*-vinylcarbazole). Poly(*N*-vinyl carbazole) was first used in electrophotography due to its high degree of photoconductivity, and then later in the field of photocopying.[33] Carbazole derivatives have also seen much attention in the field of organic light emitting diodes (OLEDs) and dye-sensitized solar cells (DSSCs) due to their ability to allow charge transfer processes to occur. In particular, the ability of carbazolyl groups to serve as either a peripheral donor or a π-linker allow flexibility in its uses.[34] Some of the reasons that carbazolyl groups are so commonly used in a variety of fields include the ease of introducing substituents into the carbazole ring, their high thermal and photochemical stability, and the ease of acquiring carbazole from coal-tar distillations.[33]

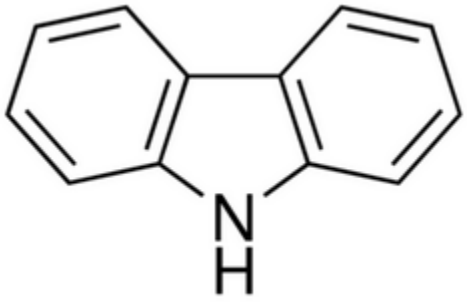

Scheme 2-1: Structure of carbazole

One of the most commonly used carbazole derivatives is its dimer, bicarbazole (BCBZ). Bicarbazole is readily produced from the oxidation of carbazole. It is believed that when carbazole undergoes oxidation, a carbazolium radical cation is generated as an electron is extracted from the molecule. This cation is highly unstable, and rapidly dimerizes, forming bicarbazole. However, there is some uncertainty as to the true mechanism behind this reaction[35]. While the first step is generally agreed upon, it is difficult to observe these species, due to the short lifetime and high reactivity the carbazolium ions display[36,37]. For the dimerization step, numerous methods have been attempted to study this reaction, including cyclic voltammetry[36], rotating disk voltammetry,[37] and electron spin resonance spectroscopy. It was proposed that the dimerization step would take place between two of the radical carbazolium molecules, so the final step would be a radical-radical reaction (Scheme 2-2, Route A)[36]. However, the evidence for this is not fully-conclusive, and the two radical cations would need to overcome Coulombic repulsion in the process of dimer formation. In addition, by using mass spectrometry to analyze this reaction, more information about the reaction

intermediates could be obtained, thanks to the high specificity of mass spectrometry, as well as the ability to perform tandem mass spectrometry to obtain structural information. The coupling of electrochemistry with mass spectrometry (EC-MS) has been shown to be particularly powerful in the elucidation of reaction mechanisms by utilizing the ability of MS to detect reaction intermediates[38,39,40,41,42], due to the ease of comparing spectra obtained both with and without the influence of oxidation, as well as the relatively short delay between oxidation and detection that can be afforded.

In our lab, we have focused on the development of a variety of techniques for the coupling of electrochemistry with mass spectrometry to detect reaction intermediates. First, we were able to couple electrochemistry with desorption electrospray ionization mass spectrometry (EC-DESI-MS) to observe the generation of the carbazolium radical cation following oxidation. We also investigated the dimerization pathway and propose that bicarbazole is produced by the reaction of a radical carbazolium with a neutral carbazole (Scheme 2-2, Route B), not the two radical carbazoliums that was previously proposed (Scheme 2-2, Route A). Due to the importance of carbazole and its derivatives, determining the correct mechanism of dimerization can be of high importance to the understanding of carbazole polyermization. This work was performed in collaboration with Dr. Chengyuan Liu from the University of Science and Technology of China.

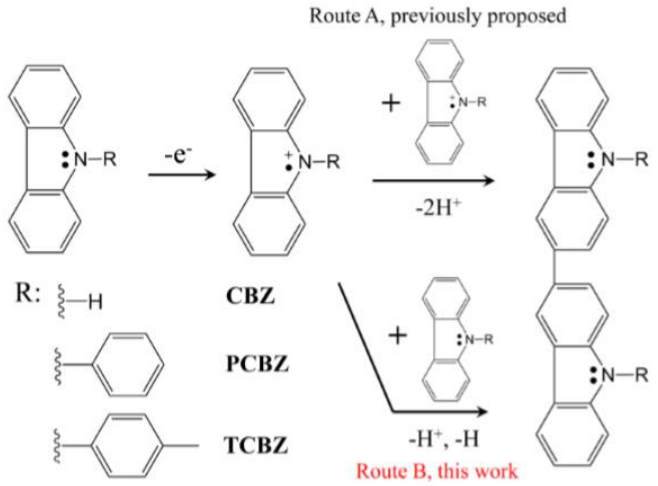

Scheme 2-2: Comparison of proposed mechanisms for carbazole oxidation and subsequent dimerization.

2.2 Carbazole Apparatus

The mass spectrometer used in these experiments was the Q Exactive Plus hybrid quadrupole-Orbitrap mass spectrometer (Thermo Fisher Scientific, San Jose, CA). Generally, the ionization source supplied with the MS was removed, and replaced with a homemade ionization source. For the homemade source, a piece of fused silica capillary (100 µm i.d., 198 µm o.d.) was used to deliver the sample solution from a syringe (Hamilton, CA) to the ionization source. This ionization source is readily interfaced with electrochemical cells via a piece of silica capillary, allowing online EC/MS experiments. A generalized form of this apparatus, showing the interface between the silica capillary, the ionization source, and mass spectrometer is shown in Scheme 2-3. The silica capillary can be directly connected to the EC cell.

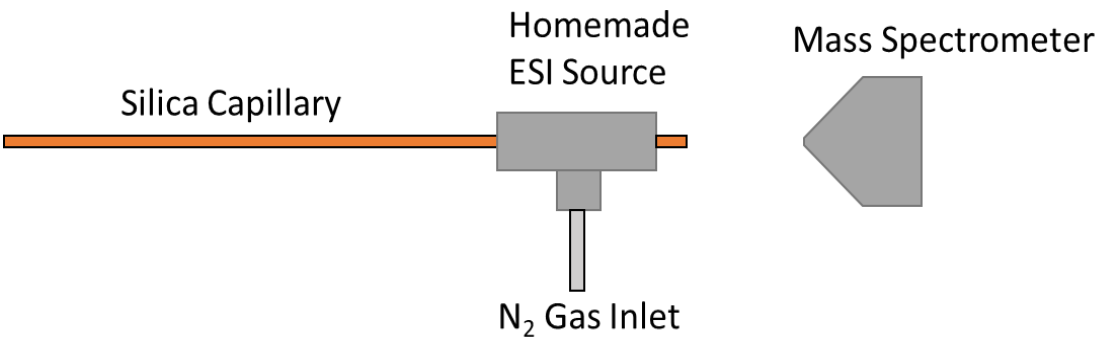

Scheme 2-3: Generalized form of the apparatus used for MS experiments. The silica capillary is connected to a syringe, which injects liquid. Sample is ionized at the ESI source and detected by the mass spectrometer.

In some experiments to offline analyze electrogenerated species from cell, nano-electrospray ionization (nESI) was used in place of the previously mentioned ionization source. In nESI, a fused silica capillary (100 µm original i.d., 198 µ.m. od) is first pulled by a laser puller to produce a long, tapered tip with an i.d. of approximately 10-20 µm. For nESI, no assisting gas flow is necessary due to the tapering of the capillary, and a high potential is applied (typically 2500V), along with a very low flow rate (typically <2 µL/min).

2.2.1 Waterwheel Set-up

First, the initial oxidation step of carbazole to the carbazolium radical cation was examined using a waterwheel set-up (Scheme 2-4). Using this set-up, sample solution of 1 mM CBZ in 1:1 MeOH/H_2O with 1% formic acid was injected into the ionization source at a flow rate of 50 µL/min. To assist in ionization, a nebulizing gas of 180 psi was used, while no high voltage was applied to the solution to avoid in-source oxidation. The source was angled such that it would spray onto a rotating Platinum disk, serving as the working electrode, which was connected to a low voltage brush-type DC motor. The

disk was immersed in a reservoir of 9:1 H_2O/MeCN containing 1 mM of ammonium acetate as electrolyte. As the disk rotates (1 rev/s), a thin layer of reservoir solution (ca. 1 mm thick) forms on the working electrode. A silver/silver-chloride reference electrode as well as a carbon cloth counter electrode were also immersed in the reservoir, and all three electrodes were connected to a CV-27 potentiostat (Bioanalytical Systems, West Lafayette, IN) which was capable of applying a potential across the system. The working electrode was then positioned approximately 2 mm for the mass spectrometer inlet. As carbazole solution was sprayed onto the electrode, it could undergo oxidation (+2.0V) before entering the inlet for detection.

This experiment was also repeated for two *N*-substituted carbazole derivatives, 9-(p-tolyl)carbazole (TCBZ) and 9-phenylcarbazole (PCBZ). In these experiments, the flow rate of injection was decreased to 20 μL/min, while all other parameters were kept the same.

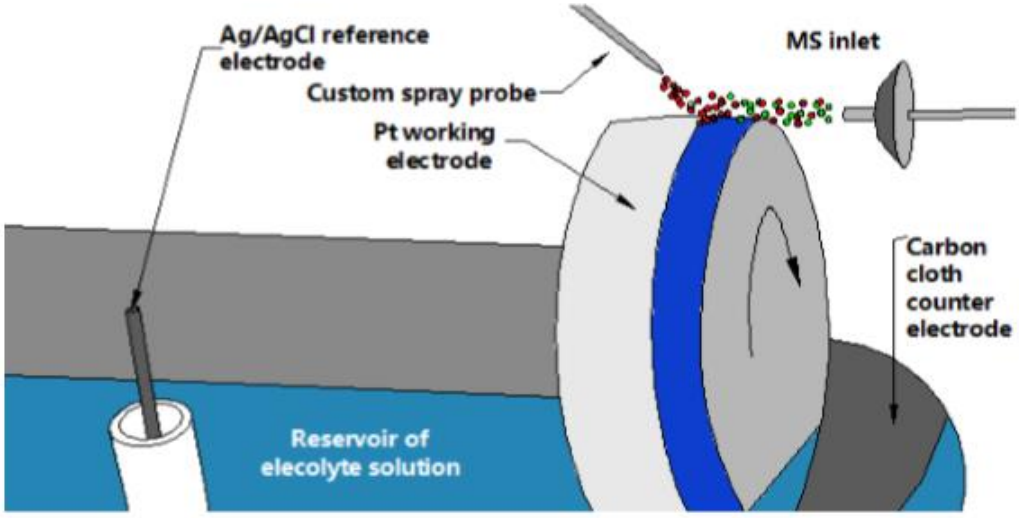

Scheme 2-4: Waterwheel set-up used in this experiment. The custom spray probe carrying analyte solution is directed at the platinum working electrode, where it undergoes oxidation before traveling into the MS inlet.[43]

2.2.2 Mixing Set-up

To investigate the dimerization step of carbazole, an isotopic mixing step was introduced prior to ionization (Scheme 2-5). In this set-up, carbazole (0.5 mM in MeCN) was injected into the system using a piece of fused silica capillary, traveling through a thin-layer electrochemical flow cell equipped with a glassy carbon working electrode (30x12 mm^2, ANTEC BV, the Netherlands, connected to an ANTEC ROXY potentiostat) that was then connected to a tee junction. At this junction, a second line of solution was infused in parallel, which could contain either solvent (MeCN) or the deuterated form of carbazole, carbazole-d_8 (0.5 mM in MeCN). These two solutions would then mix and exit the tee junction together, at which point the resulting mixture could either be collected or directly undergo ionization. The benefit of this set-up is that only the first solution undergoes oxidation, so that only radical cations of carbazole-d_0 should be generated.

Under a radical-radical reaction mechanism to form dimer, this should result solely in the formation of bicarbazole-d_0. However, if the reaction mechanism is radical-neutral, it should be possible to observe the deuterated forms of bicarbazole as well. The flow rate for both solutions was 70 µL/min, and an oxidation potential of +2.0V was used.

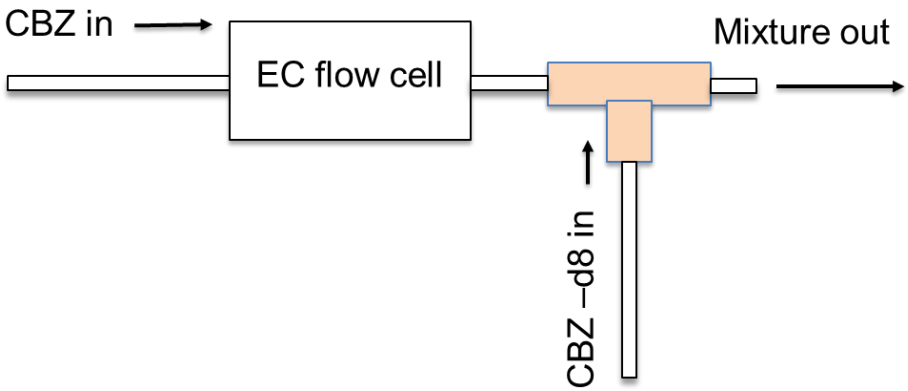

Scheme 2-5: Apparatus used for the analysis of the carbazole dimerization. Carbazole solution flows through an electrochemical flow cell, where it then enters into a tee junction and mixes with separately introduced carbazole-d_8 solution. The combined mixture then exits the tee junction.

2.3 Results and Discussion of Carbazole

2.3.1 Electrochemical Oxidation of Carbazole

First, the initial oxidation step of carbazole was investigated. Previously, the detection of the carbazolium radical cation has been difficult to accomplish. It had previously been thought to have been observed in 1965[44], but later work cast doubt on whether it was the actual species detected[45]. The radical cation of PCBZ was observed by electron-transfer stopped flow absorption spectroscopy[46], and the radical cation of CBZ was detected using luminescence spectroscopy[47]. Mass spectrometry is an attractive technique to attempt to detect this species, due to its high specificity. To detect these

radical cations, the waterwheel set-up previously mentioned was used (Scheme 2-4). For carbazole, 1 mM carbazole solution in 1:1 MeOH/H_2O with 1% formic acid was injected into the ionization source at a flow rate of 50 μL/min and directed towards the rotating disk electrode set-up, described previously. When no potential was applied to the electrode (Figure 2-1A), a peak at *m/z* 168.0803 was observed, which corresponds to the protonated cation of carbazole ($[CBZ+H]^+$, theoretical mass: *m/z* 168.0808, mass error: 3.0 ppm), as well as a much smaller peak at *m/z* 167.0725, believed to correspond to the carbazolium radical cation ($[CBZ^{\bullet}]^+$, theoretical mass: *m/z* 167.0730, mass error: 3.0 ppm). This small peak may be due to the common occurrence of in-source oxidation during the ionization process[48]. When an oxidation potential of +2.0V was applied to the rotating electrode (Figure 2-1B), a near ten-fold increase in the peak intensity of *m/z* 167.0725 was observed, supporting its assignment as the carbazolium radical cation peak. As the potential was varied on and off, the peak intensity continued to fluctuate, as shown in its extracted ion chromatogram (EIC, shown in Figure 2-1C), supporting its assignment as the carbazolium radical cation.

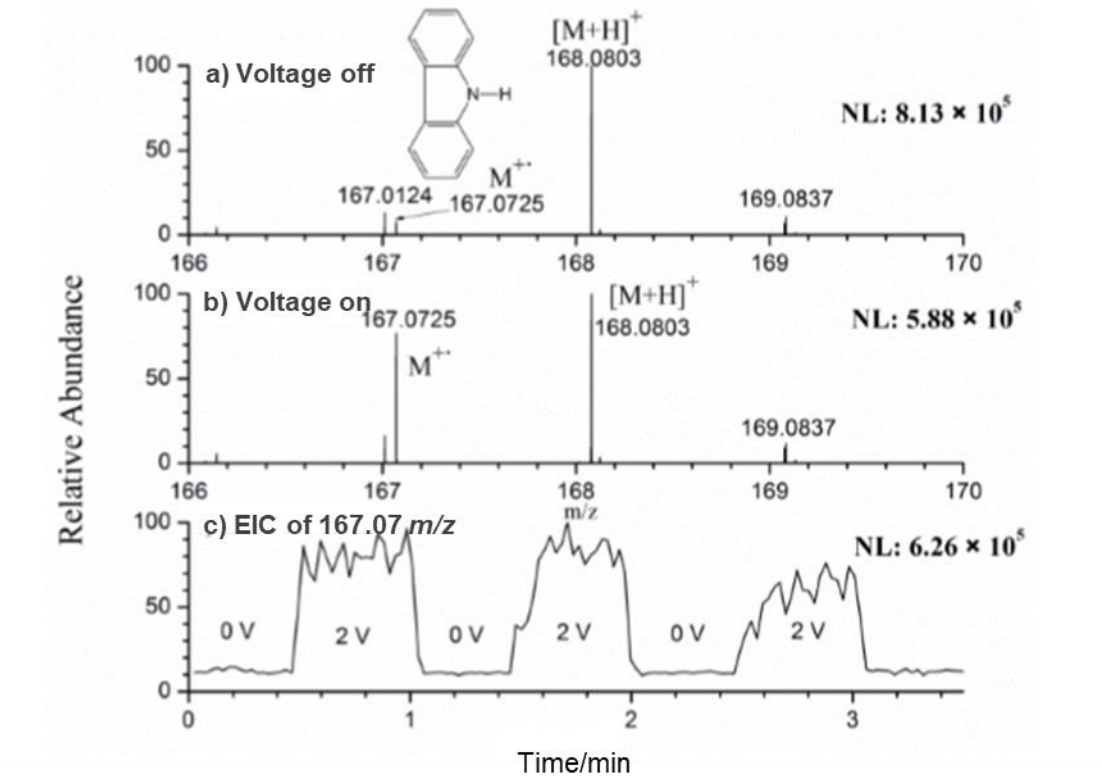

Figure 2-1: A.) MS spectrum of carbazole using waterwheel set-up with no applied potential; B.) MS spectrum of carbazole using waterwheel set-up when +2.0V is applied to the rotating electrode; C.) EIC of *m/z* 167.0725 showing fluctuation in peak intensity as oxidation potential is switched off and on.

In addition to the observation of the radical cation, 3,3'-bicarbazole formation was also observed. Following ionization, standard 3,3'-bicarbazole is typically observed as a radical cation ([BCBZ $^{\bullet}$]$^{+}$), with a theoretical mass of *m/z* 332.1308. When no potential was applied to the system (Figure 2-2A), no corresponding peak was observed. However, when the potential was switched on (Figure 2-2B), a peak at *m/z* 332.1296 was observed ([BCBZ $^{\bullet}$]$^{+}$, theoretical mass: *m/z* 332.1308, mass error: 3.3 ppm), corresponding to the formation of dimer. Indeed, the EIC of this peak (Figure 2-3C)

closely matches that of *m/z* 167.0725, indicating that the formation of the two are both linked and both due to oxidation, as expected.

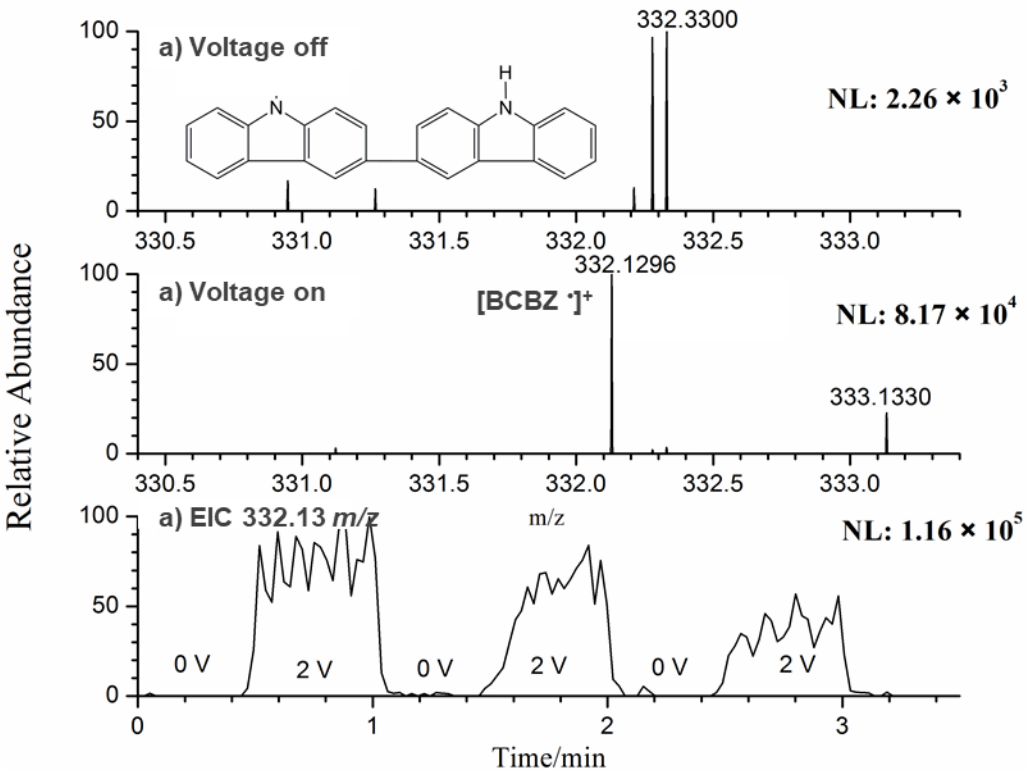

Figure 2-2: A.) MS spectrum of carbazole using waterwheel set-up with no applied potential; B.) MS spectrum of carbazole using waterwheel set-up when +2.0V is applied to the rotating electrode; C.) EIC of *m/z* 332.1296 showing fluctuation in peak intensity as oxidation potential is switched off and on.

To verify the status of the observed peaks at *m/*z 167.0725 and *m/z* 332.1296 as genuine carbazolium and 3,3'-bicarbazole radical cations, collision induced dissociation (CID) analysis of the peaks was applied. In the fragmentation of *m/z* 167.0725, two major resulting peaks were observed: one at *m/z* 166.06 indicating the loss of H, likely from the amine group; and the second at *m/z* 140.06, proposed to be from the loss of -HCN (Figure 2-3A). For 3,3'-bicarbazole radical cation, the CID data obtained from the generated *m/z*

332.1296 (Figure 2-3B) was compared to that of the authentic 3,3'-bicarbazole radical cation (Figure 2-3C). Both spectra showed the same fragmentation patterns such as losses of H, 2H, and C_2H_2, confirming the ion assignment.

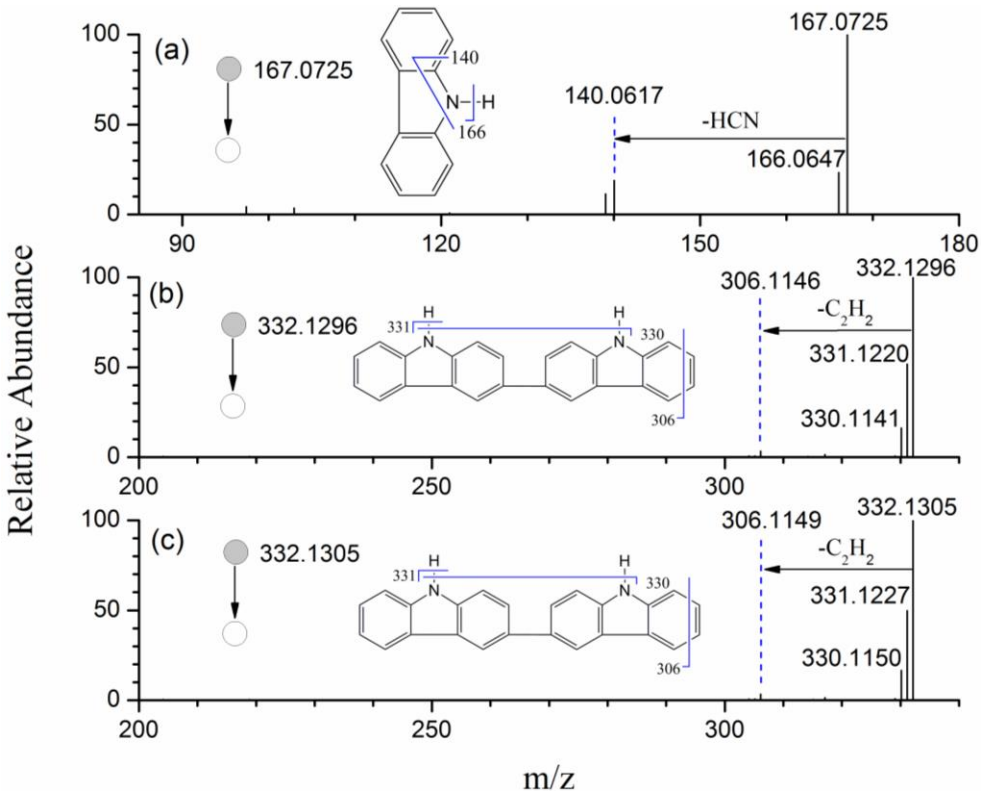

Figure 2-3: A.) CID MS/MS spectrum for generated *m/z* 167.0725 following oxidation; B.) CID MS/MS spectrum for generated *m/z* 332.1296 following oxidation; C.) CID MS/MS spectrum for peak at *m/z* 332.1305 for authentic 3,3'-BCBZ sample.

Similar experiments were performed for both PCBZ and TCBZ. In both, similar results were observed, with the formation of both $[PCBZ^{\bullet}]^+$ and $[TCBZ^{\bullet}]^+$ when oxidation potential was applied to the electrode.

2.3.2 Elucidation of Dimerization Mechanism

As mentioned, there is considerable doubt as to the true mechanism which drives the dimerization reaction. Therefore, designing a method to provide clear evidence one way or the other is quite challenging. To tackle this problem, isotopic labeling experiments were performed, which we have previously used for analyzing complex reactions[49]. In this case, the deuterated form of carbazole, carbazole-d_8 would be mixed with non-deuterated carbazole following its oxidation. If the reaction required two radical carbazolium ions to take place, it is predicted that only the non-deuterated 3,3'-bicarbazole would be detected. However, if the reaction involves a neutral parent molecule, it would then be possible for a carbazolium ion generated for the non-deuterated carbazole to react with a carbazole-d_8 molecule, generating a heterodimer 3,3'-bicarbazole-d_7. To test this, the mixing set-up (Scheme 2-5) described previously was used. Carbazole was infused through an electrochemical flow cell and oxidized with a potential of +2.0 V. In parallel to this, either solvent (MeCN) or carbazole-d_8 would be introduced, such that they would mix with the carbazole solution shortly after oxidation. After mixing, the resulting solution was collected and then analyzed via nano-ESI, with a sample flow rate of 1 µL/min and an applied potential of +2500V to assist in the ionization process. When solvent was mixed with carbazole (Figure 2-4A), a large peak at *m/z* 332.1302 was observed, corresponding to $[BCBZ^{\bullet}]^+$ (theoretical mass: *m/z* 332.1308, mass error: 1.8 ppm), while no peak was observed corresponding to $[BCBZ\text{-}d_7^{\bullet}]^+$ (theoretical mass: *m/z* 339.1747). This is the expected result when solvent is mixed with oxidized carbazole. When carbazole-d_8 was mixed with carbazole (Figure 2-4B), a

new peak at *m/z* 339.1744 was observed, corresponding to [BCBZ-d_7 •]$^+$ (theoretical mass: *m/z* 339.1747, mass error: 0.88 ppm). This presence of this peak indicates the ability of the generated carbazolium radical cations to react with the neutral carbazole-d_8 which was introduced independently, supporting a radical-neutral mechanism. One potential problem with this set-up is the short lifetime of the carbazolium radical cation, as that means the amount of radical cation surviving until mixing with the deuterated form is very low, leading to a small peak for the deuterated 3,3'-bicarbazole.

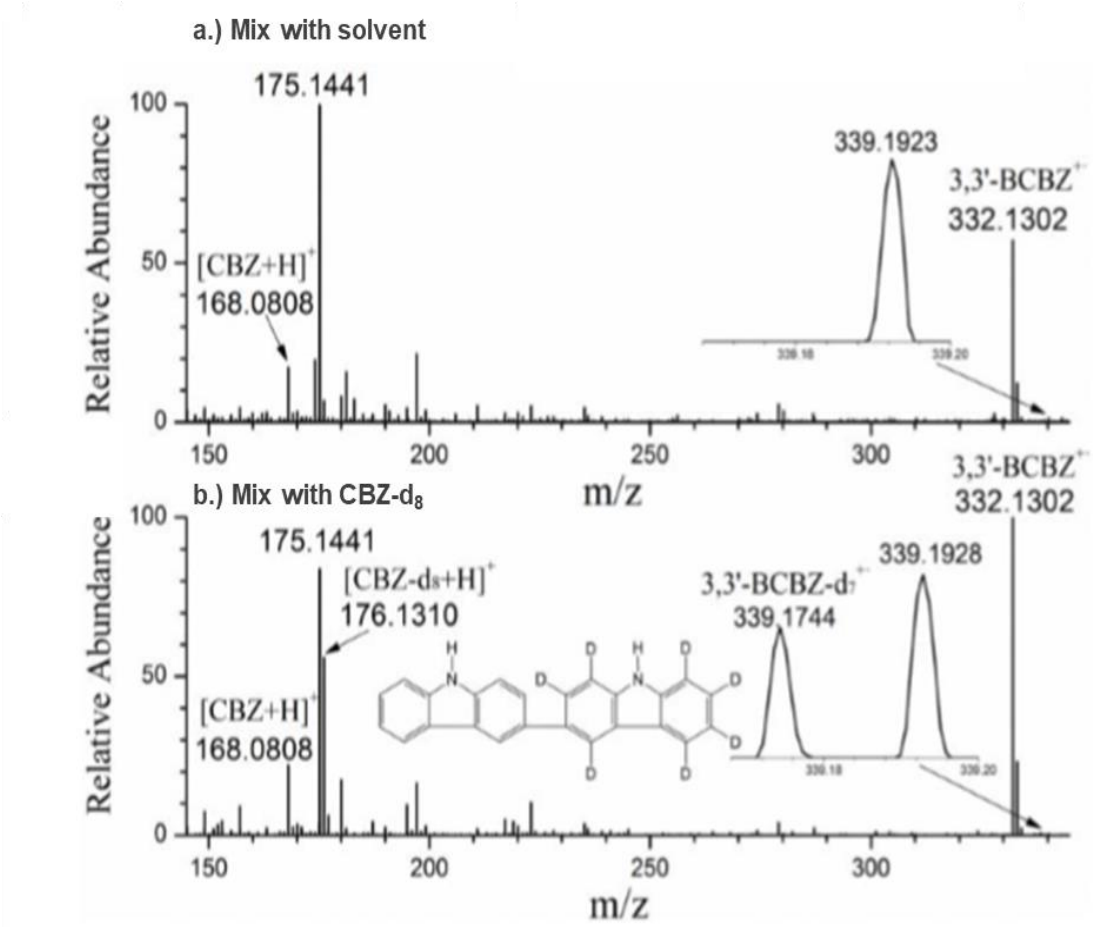

Figure 2-4: A.) nESI-MS spectrum of CBZ oxidation followed by mixing with MeCN; B.) nESI-MS spectrum of CBZ oxidation following by mixing with CBZ-d_8

This experiment was repeated (Figure 2-5) wherein a high mixing flow rate (70 µL/min) was used and the distance needed for the oxidized carbazole to travel prior to mixing was reduced. It was observed that when CBZ underwent oxidation, both BCBZ and BCBZ-d_7 were observed in better intensity (Figure 2-5B), while no BCBZ-d_{14} was present. When CBZ-d_8 was the compound oxidized (Figure 2-5C), the reverse was true. This would indicate that the reaction may be proceeding by a radical-neutral mechanism, as under a radical-radical mechanism it would be expected for BCBZ-d_{14} to be observed, even if in relatively small amounts compared to the peak for BCBZ-d_0.

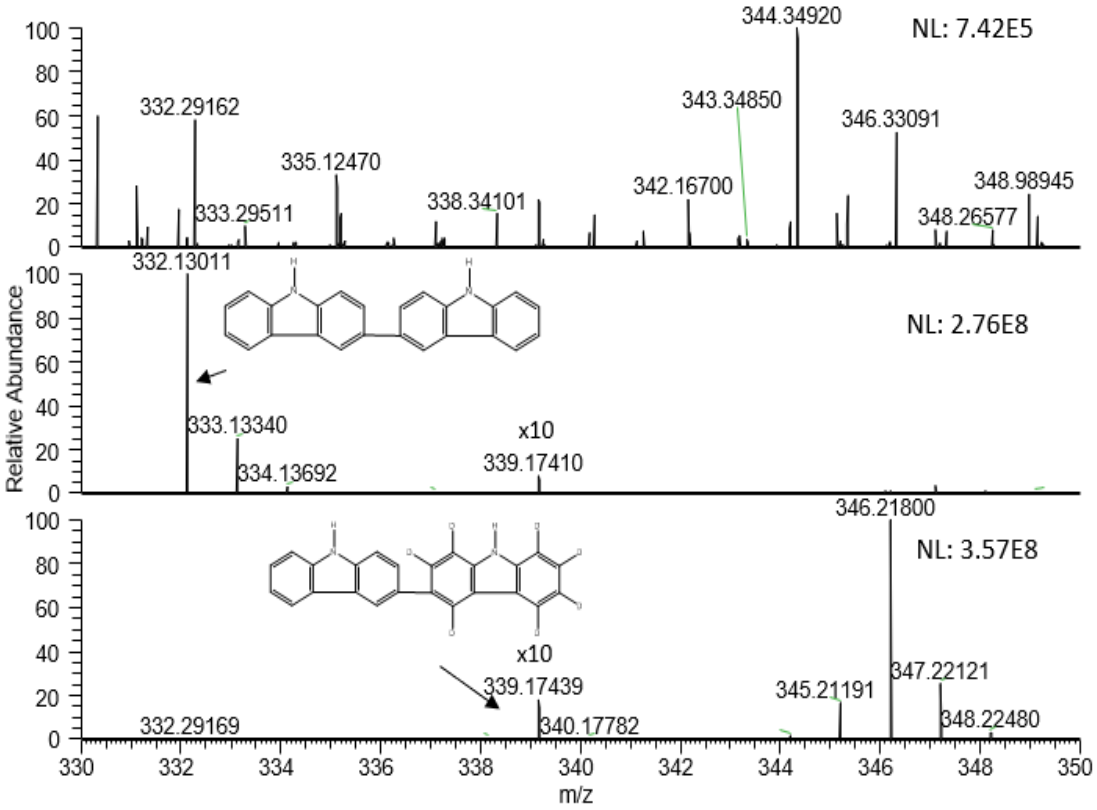

Figure 2-5: Dimer peaks observed when A.) neither CBZ nor CBZ-d_8 was oxidized, B.) CBZ was oxidized, and C.) CBZ-d_8 was oxidized. The peak at *m/z* 339.174 is magnified by a factor of 10 for clarity.

2.4 Introduction to Triphenylamine

Triphenylamine, structurally similar to carbazole, is also an aromatic amine, with many of the same uses. One major field in which triphenylamine is used in is as a dye in dye-sensitized solar cells (DSSCs). Triphenylamine based dyes hold the record for being the most efficient among metal-free organic dyes, with an efficiency over 10.3%, due to its status as well-performing electron donor and its non-planar structure preventing aggregate formation.[50] In addition, triphenylamines have found use in the field of optoelectronics as a hole transport material. Recently, work with triphenylamine dimers has also shown their potential for use as an organic field-effect transistor in the development of circuits in place of silica, particularly when the produced dimers are cyclical in nature[52]. However, their field of uses is quite broad, and includes the design of polymers, polyradicals, and pharmaceuticals[52]. In parallel to carbazole, triphenylamine is also believed to undergo a two-step dimerization process: first the loss of an electron due to oxidation, followed by dimerization[53]. While pulse-electrolysis stopped flow data shows that the reaction mechanism to form dimer requires two radical species to proceed[53], it may be also worth investigating by mass spectrometry.

2.5 Triphenylamine Apparatus

The mass spectrometer used in these experiments was the Q Exactive Plus hybrid quadrupole-Orbitrap mass spectrometer (Thermo Fisher Scientific, San Jose, CA). Generally, the ionization source supplied with the MS was removed, and replaced with a homemade ionization source. For the homemade source, a piece of fused silica capillary (100 μm i.d., 198 μm o.d.) was used to deliver the sample solution from a syringe

(Hamilton, CA) to the ionization source. For these experiments, no potential was applied to the sample, to avoid the influence of in-source oxidation, and a nebulizing gas of 180 psi was used. For the electrochemical cell set-up, a modified BASi electrochemical flow cell was used. Instead of having both an inlet and outlet for the cell, both were used as inlets for two parallel solutions (Scheme 2-6). Then, the injected solution would pool in the reservoir for the reference electrode, which was removed from the cell. This allows for very short delay prior to mixing of the two electrolyzed solutions, allowing us to investigate the reactivity of TPA radical cations in details. For the working electrode, two small, round, glassy carbon electrodes (diameter = ~0.4 cm) were placed into a PEEK block spaced 0.25 cm apart, with the outlet to the reference electrode reservoir between them (no reference electrode was used in this experiment). Typically, a flow rate for both solutions being infused into the cell was set at 40 μL/min. The purpose of this was to reduce the delay between oxidizing and mixing, to increase the amount of dimer formed.

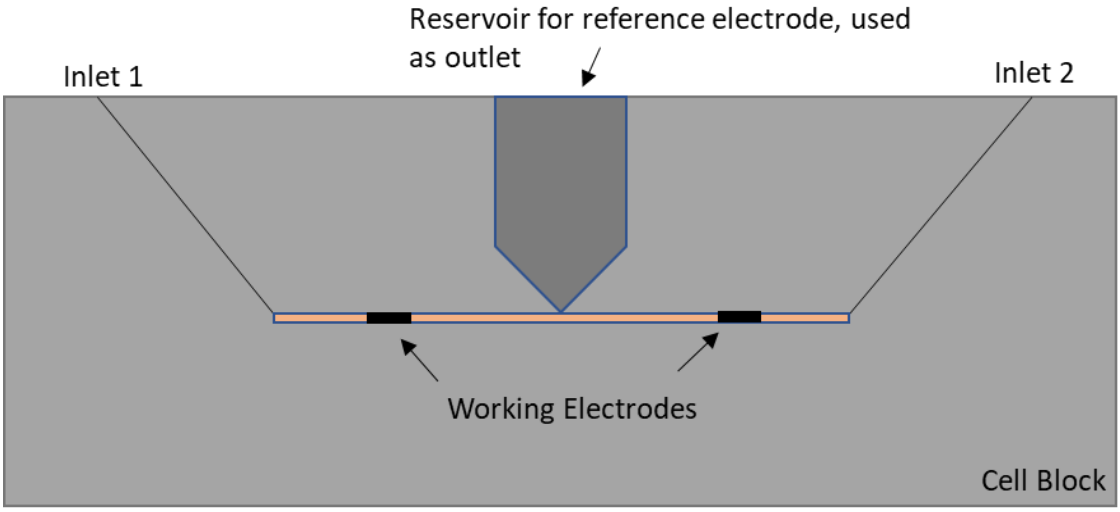

Scheme 2-6: Design of a cell block used for TPA experiments. The two TPA compounds, TPA and TPA-d15, are introduced separately through the two inlets, then travel over the two working electrodes before mixing and exiting through the reference electrode reservoir.

2.6 Results and Discussion of Triphenylamine

2.6.1 Detection of Triphenylamine Radical Cation by MS

The radical cation of triphenylamine could be detected by MS. Using SSI and the oxidation set-up shown in Scheme 2-6, 200 µM of TPA-d_{15} was oxidized and mixed with 200 µM of TPA. When the mixture was analyzed by MS (Figure 2-6, it was observed that a significant amount of $[TPA\text{-}d_{15}^{\bullet}]^{+}$ was observed at *m/z* 260.21451 (theoretical mass: *m/z* 260.21405, mass error: 1.76 ppm), while no radical cation of TPA was observed (theoretical mass: *m/z* 245.11990).

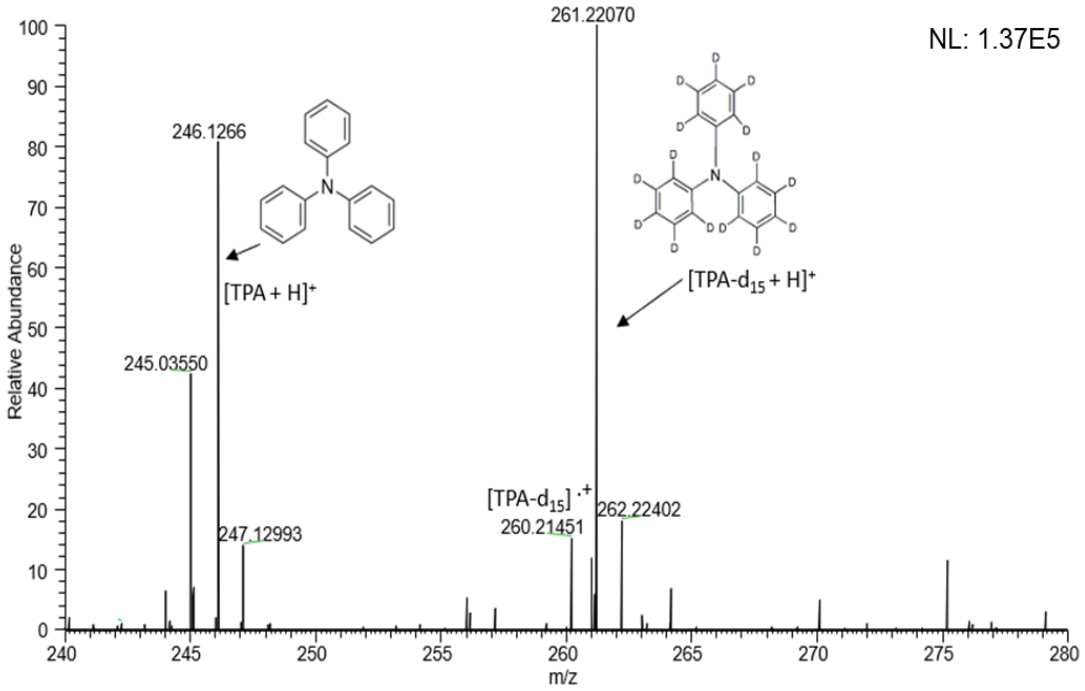

Figure 2-6: Acquired mass spectrum of TPA and TPA-d_{15} when TPA-d_{15} undergoes oxidation

2.6.2 Isotope Labeling Experiments

Like carbazole, isotopic labeling was used to investigate the mechanism of TPA dimerization, by mixing triphenylamine with triphenylamine-d_{15}, resulting in the formation of *N,N,N*'-triphenylbenzidine (TPB). Depending on which of the two triphenylamine species are oxidized, three different potential dimer peaks should be observed: TPB-d_0, with a theoretical mass of *m/z* 488.22; TPB-d_{14}, with a theoretical mass of *m/z* 502.31; and TPB-d_{28}, with a theoretical mass of *m/z* 516.40. Unlike carbazole however, in-source oxidation seems to be much more prevalent for TPA, leading to non-insignificant amounts of radical cation for the TPA monomers, as well as influencing the formation of dimer. To help understand the data, the proposed pathway

by which certain peaks would be formed, as well as how the relative intensity of how those peaks should appear was first determined.

Under a radical-neutral mechanism when triphenylamine is oxidized (Scheme 2-7a), the first step should always be the loss of an electron from [TPA], leading to the formation of $[TPA^{\bullet}]^{+}$. Then, it should be highly likely that the formed $[TPA^{\bullet}]^{+}$ should react with the non-oxidized [TPA], leading to a large amount of TPB-d_0. It is also likely, due to the relatively short delay between oxidation and mixing, that the remaining $[TPA^{\bullet}]^{+}$ will be able to react with [TPA]-d_{15}, forming a good amount of TPB-d_{14}. However, to form TPB-d_{28}, it is necessary for a charge transfer step to occur, as $[TPA^{\bullet}]^{+}$ must impart its charge onto a neutral TPA-d_{15}, resulting in the formation of $[TPA^{\bullet}\text{-}d_{15}]^{+}$, which must then react with a neutral TPA-d_{15} to form TPB-d_{28}. This should lead to high peaks at *m/z* 488.22 and *m/z* 502.31, but a low peak at *m/z* 516.40, if one is present at all.

A.) Radical-Neutral Mechanism

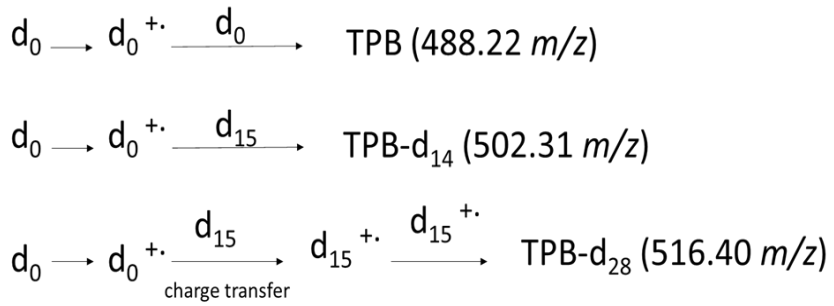

B.) Radical-Radical Mechanism

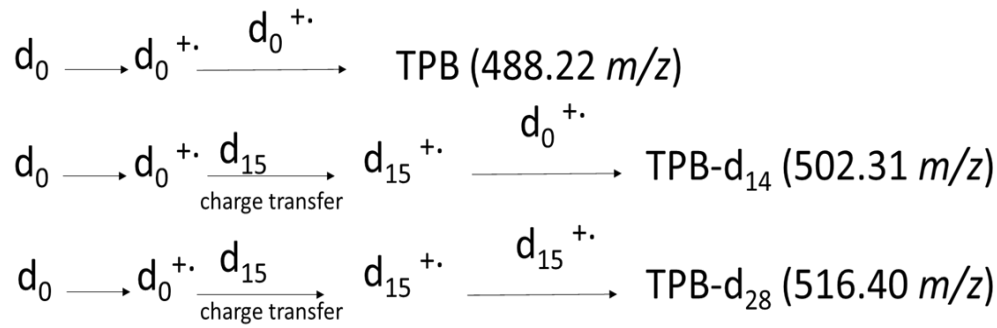

Scheme 2-7: Proposed pathways for the formation of different dimers if pathway proceeds via a) a radical-neutral mechanism and b) a radical-radical mechanism.

The results if a radical-radical mechanism was correct were also proposed (Scheme 2-7b). Under a radical-radical mechanism, the formation of non-deuterated dimer should be highly favored, as only the non-deuterated form of TPA undergoes oxidation in our experiment. To from TPB-d_{14} or TPB-d_{28}, one or two charge transfer steps are respectively required, which are believed to be less favorable or likely than simply forming dimer.

To test these hypotheses, TPA and TPA-d_{15} were mixed as described. In addition, the relative concentration of the two species were varied, to investigate the impact that would have on the resulting mixture. Initially, the concentration of both monomeric

species was 200 μM. When the two were mixed with no oxidation taking place, a small peak which could correspond to TPB was potentially observed, but no peaks for TPB-d_{14} or TPB-d_{28} were found (Figure 2-7A). When the two species were mixed at a 1:1 ratio and TPA was oxidized (Figure 2-7B), the resulting spectra showed a dominant peak at *m/z* 488.2231, believed to correspond to $[TPB^{\bullet}]^{+}$ (theoretical mass: *m/z* 488.2247, mass error: 3.27 ppm), as well as a peak with roughly half of its intensity at *m/z* 502.3106, corresponding to $[TPB\text{-}d_{14}^{\bullet}]^{+}$ (theoretical mass: *m/z* 502.3126, mass error: 3.98 ppm) and a smaller peak at *m/z* 516.3984, corresponding to $[TPB\text{-}d_{30}^{\bullet}]^{+}$ (theoretical mass: *m/z* 516.4004, mass error: 3.87 ppm). When the concentration of the two monomeric species was then varied to 1:2 TPA:TPA-d_{15} by reducing the concentration of TPA to 100 μM, the spectra shifted, with a relative increase of *m/z* 502.3114 such that it is now the highest of the dimer peaks (Figure 2-7C). When the concentration was reversed, with a 2:1 ratio of TPA:TPA-d_{15} and TPA-d_{15} now at 100 μM (Figure 2-7D), the peak at 502.3114 *m/z* falls below its previous relative intensity from when the two species were mixed 1:1. Under a radical-radical mechanism, it is expected that both TPB and TPB-d_{14} peaks should undergo a similar decline when the amount of TPA is decreased from 200 to 100 μM, as both require two non-deuterated TPA as part of their pathway (for TPB, two TPA radical cations are directly required, for TPB-d_{14} one TPA radical cation is directly required and the second TPA radical cation must cause a charge transfer step to generate the necessary $[TPA\text{-}d_{15}^{\bullet}]^{+}$ to form deuterated dimer). This is not what is indicated in the data, as the relative decrease for TPB is larger than that observed for TPB-d_{14}. However, if the dimerization were to follow a radical-neutral process, no charge transfer step would

be necessary, so only one TPA radical cation would be needed to form TPB-d_{14}, and it would then be expected that the TPB-d_{14} peak should rise relative to the TPB peak, which would still require two TPA to form.

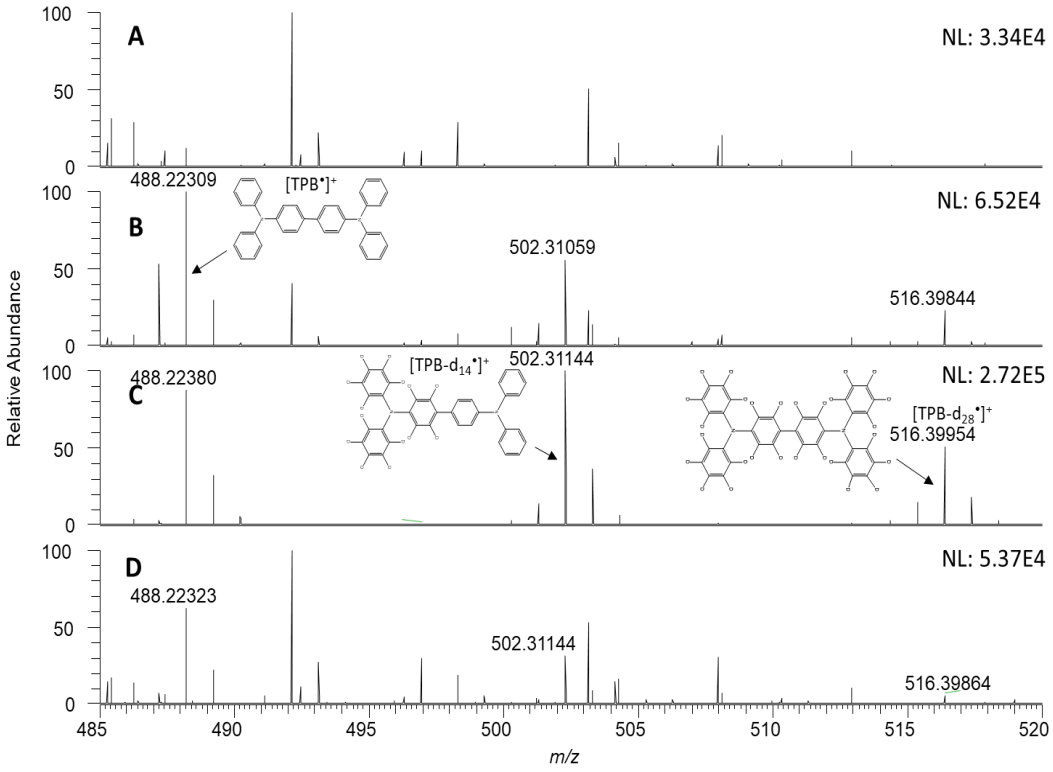

Figure 2-7: A.) MS spectrum resulting from the mixture of 1:1 TPA:TPA-d_{15} with no oxidation; B.) MS spectrum resulting from the mixture of 1:1 TPA:TPA-d_{15} when TPA is oxidized; C.) MS spectrum resulting from the mixture of 1:2 TPA:TPA-d_{15} when TPA is oxidized; D.) MS spectrum resulting from the mixture of 2:1 TPA:TPA-d_{15} when TPA is oxidized.

The reverse of these experiments, where TPA-d_{15} was the species undergoing oxidation, were also performed. Again, when the two were mixed with no oxidation taking place, very little dimer peak was observed (Figure 2-6A). When a 1:1 mixing ratio was used (Figure 2-8b), $[TPB\text{-}d_{28}^{\bullet}]^{+}$ was the dominant peak, as expected, while [TPB-

$d_{14}^{\bullet}]^+$ had a similar intensity to that seen in Figure 2-8B When TPA-d_{15} outnumbered TPA 2:1 (Figure 2-8C), the results that were seen were the reverse of that in Figure 2-5d, with $[TPB\text{-}d_{28}^{\bullet}]^+$ being the dominant peak. After the amount of TPA-d_{15} was decreased such that the ratio of TPA-d_{15} to TPA was 1:2 (Figure 2-8D), it was again observed that the $[TPB\text{-}d_{14}^{\bullet}]^+$ peak was nearly as high as that of normally dominant dimer peak from $[TPB\text{-}d_{28}^{\bullet}]^+$, further supporting a radical-neutral mechanism.

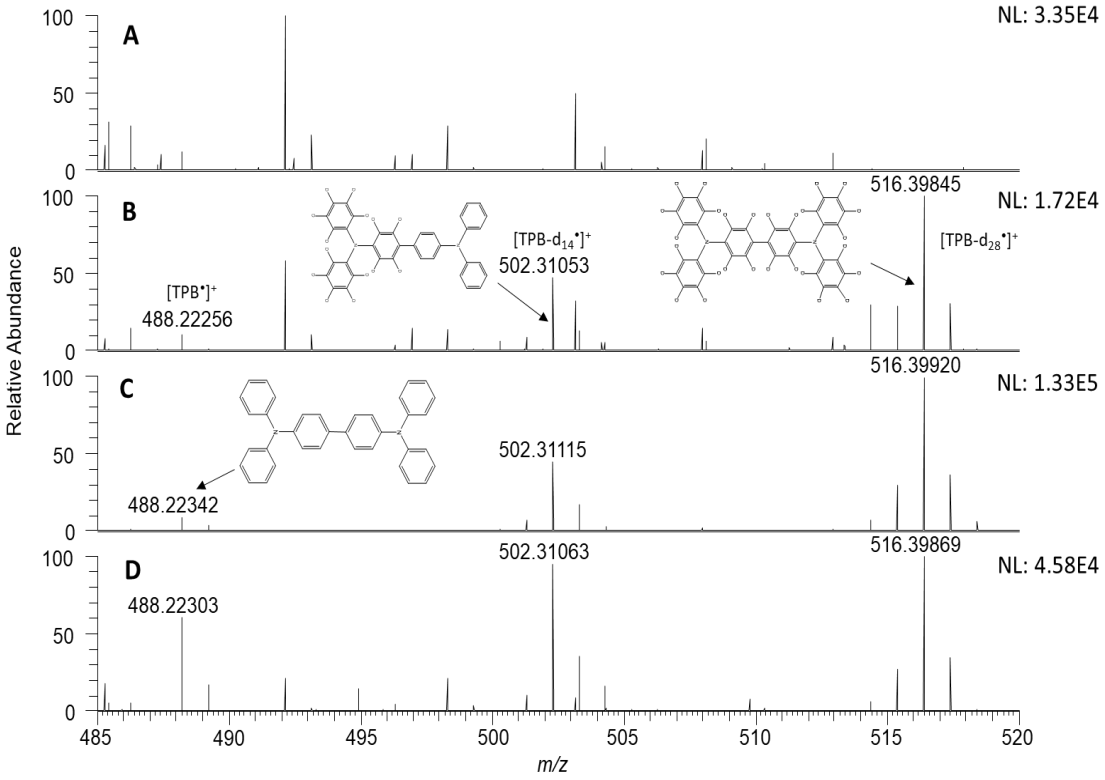

Figure 2-8: A.) MS spectrum resulting from the mixture of 1:1 TPA:TPA-d_{15} with no oxidation; B.) MS spectrum resulting from the mixture of 1:1 TPA:TPA-d_{15} when TPA-d_{15} is oxidized; C.) MS spectrum resulting from the mixture of 1:2 TPA:TPA-d_{15} when TPA-d_{15} is oxidized; D.) MS spectrum resulting from the mixture of 2:1 TPA:TPA-d_{15} when TPA-d_{15} is oxidized.

2.7 Conclusions

Using the waterwheel set-up, the carbazolium radical cation was detected by mass spectrometry, confirming the first step of the carbazole dimerization process. In addition, by introducing deuterated carbazole into the system following the oxidation of non-deutered carbazole, evidence was obtained showing the formation of deuterated 3,3'-bicarbazole, supporting a radical-neutral mechanism.

Likewise, the presence of the radical cation of triphenylamine following oxidation was also shown by mass spectrometry. Work was also done to demonstrate that the dimerization may also proceed via a radical-neutral pathway, although follow-up work to verify this may be needed.

CHAPTER 3: VISIBLE LIGHT-DRIVEN NICKEL REDUCTIVE ELIMINATION AND PYRROLIDINE DEHYDROGENATION

3.1 Introduction to Iridium-Catalyzed Photochemical Reactions

The recent renaissance in photochemistry has greatly expanded the synthetic utility and practicality of photochemical reactions[54]. Greater fundamental understanding of the reaction mechanisms of photocatalytic reactions can provide knowledge to facilitate process optimization and reaction discovery. Mass spectrometry represents a relatively simple approach that is well-suited to the study of unstable, fleeting, or poorly soluble intermediates. Development of mass spectrometry-based methodology to study photoredox reactions can provide new insights in the identification of true reaction intermediates and greater understanding of catalytic pathways. Incorporating the knowledge gained can help to improve the efficiency and reproducibility of photoredox reactions and will aid in the development of novel and superior photoredox catalysts in the future.

Recently, literature[55] has demonstrated the use of a dual catalytic cycle of a photoredox catalyst (iridium) with a transition metal catalyst (nickel), and its capabilities to allow synthetic reactions which a sole nickel catalytic system would be unable to do (Scheme 3-1A). This cycle has been shown to be capable of creating C-O and C-N bonds (Scheme 3-1B) by causing the Ni catalyst to assume a +3 state facilitating reductive elimination.[54g, 55] In the case of the amine reaction, it is proposed that two distinct single electron transfers stemming from the presence of the photocatalyst take place, the first to allow the generation of the Ni(0) species (e.g., species **3**, Scheme 3-1B) necessary to

allow the oxidative addition of an aryl bromide, and the second to later oxidize the Ni(II) species which contains both the aryl group as well as an amine to Ni(III) (e.g., species **7**, Scheme 3-1B), where it can undergo reductive elimination to form aniline derivatives, which have many uses in synthetic chemistry.[54g]

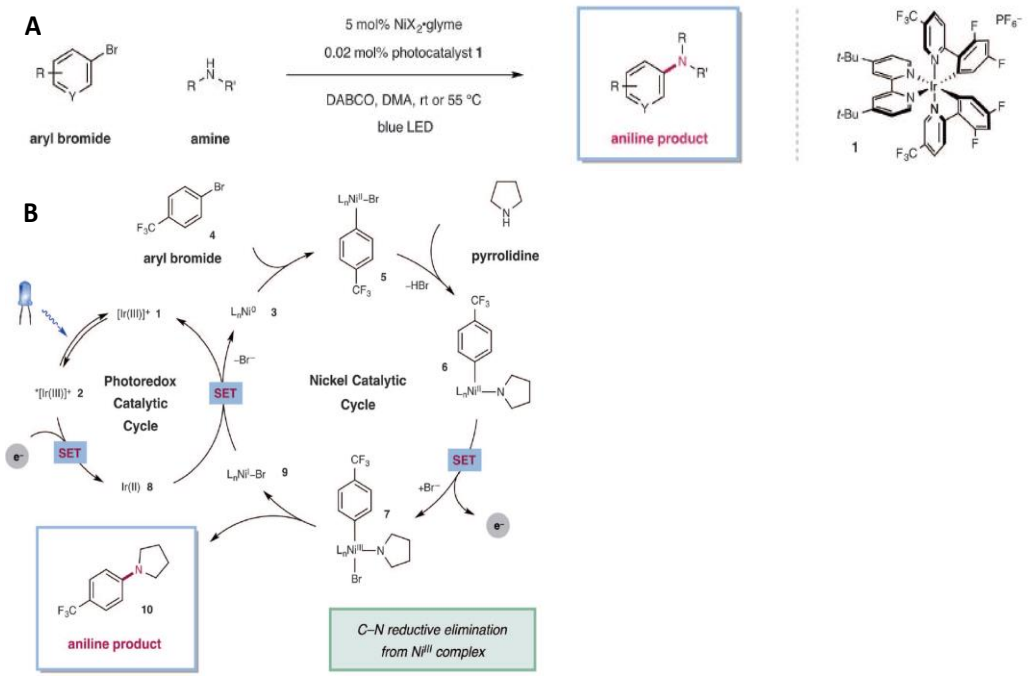

Scheme 3-1[53g]: A.) the C-N formation reaction to be studied; B.) the proposed mechanistic study.

In addition, while studying this reaction, a side reaction was observed and investigated. During the previously mentioned reaction, it was found that when pyrrolidine was used as the amine, it was possible to observe what may be a dehydrogenation reaction taking place, leading to the formation of dihydropyrrole. Pyrroles are heterocyclic compounds which are frequently used for synthetic and medicinal purposes, and often featured in porphyrin rings, which are active in

chlorophyll, heme, and vitamin B12.[56] There are numerous methods to synthesis pyrroles, however most tend most tend to involve high temperatures and more complicated reaction set-ups[57,58,59]. It is therefore possible that a light-driven reaction may then be favorable for their synthesis.

3.2 Photochemical Apparatus

The mass spectrometer used in these experiments was the Q Exactive Plus hybrid quadrupole-Orbitrap mass spectrometer (Thermo Fisher Scientific, San Jose, CA). Generally, the ionization source supplied with the MS was removed, and replaced with a homemade ionization source. For the homemade source, a piece of fused silica capillary (100 μm i.d., 198 μm o.d.) was used to deliver the sample solution from a syringe (Hamilton, CA) to the ionization source. This ionization source was readily interfaced with electrochemical cells via the silica capillary, allowing online photochemistry experiments. A generalized form of this apparatus, showing the interface between the silica capillary, the ionization source, and mass spectrometer is shown in Scheme 2-3.

In some experiments, nano-electrospray ionization was used in place of the previously mentioned ionization source. In nESI, a fused silica capillary (100 μm original i.d., 198 μ.m. od) is first pulled by a laser puller to produce a long, tapered tip with an i.d. of approximately 10-20 μm. For nESI, no assisting gas flow is necessary due to the tapering of the capillary, and a high potential is applied (typically 2500V), along with a very low flow rate (typically <2 μL/min).

In these experiments, a blue light source was used for irradiation. For nESI-MS and ESI-MS, a blue laser pointer (λ = 403 nm, 50 mW, LaserPointerPro, HK) was used,

and the laser status was toggled between off and on at regular intervals, typically every 30 s. For the online mixing set-up, a blue LED plate was used (λ = 465 nm), and the sample was constantly stirred and irradiated, with spectra being acquired every 10 min.

3.2.1 Nanoelectrospray Set-up

For nano-ESI-MS (Scheme 3-2A), the syringe was directly connected to a nano-capillary, where the coating on the tip of the capillary was removed as part of the process of pulling the capillary. This serves as an irradiation window, and the laser pointer was positioned approximately 1 cm away from the tip.

3.2.2 Electrospray Set-up

For ESI-MS (Scheme 3-2B), the syringe was connected to a piece of silica capillary which was connected to the homemade ionization source previously described. An irradiation window was created by burning the organic coating off the silica capillary immediately prior to the ionization source, and the laser pointer was positioned approximately 1 cm away from the window.

3.2.3 Online Mixing Set-up

In the online mixing set-up, unreacted sample was placed into a glass vial which was then placed on top of a blue LED array and stir plate. A silica capillary was inserted through the septum of the vial into the solution, and the other end was attached to the homemade ionization source. As N_2 travels out of the source towards the MS, the pressure difference between the vial (1 atm) and the source (lower than 1 atm due to the Venturi effect due to the blow of the sheath gas) causes solution to be pulled into the capillary, where it can be ionized and detected using SSI-MS.

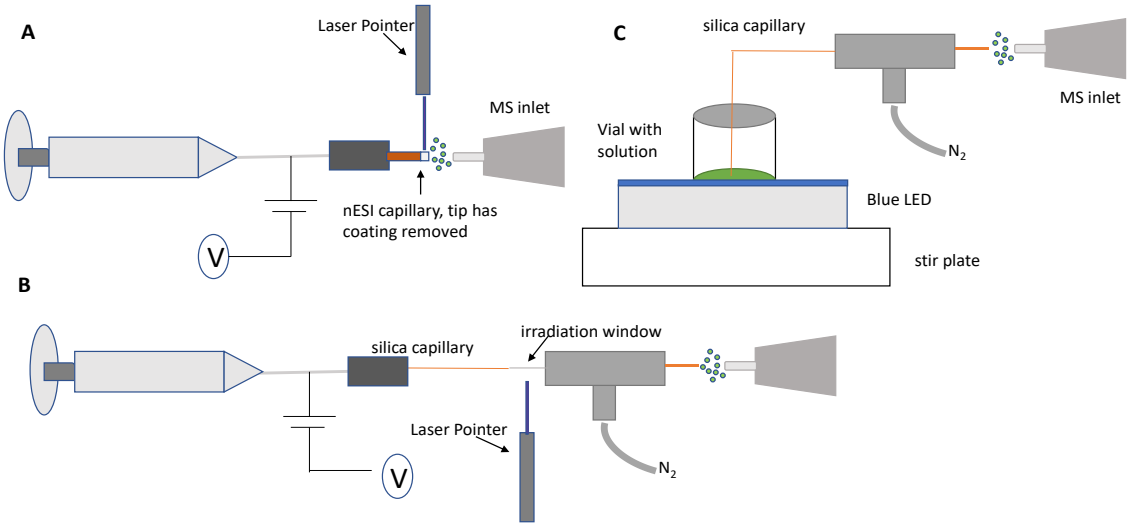

Scheme 3-2: A.) nano-electrospray set-up used; B.) electrospray set-up used; C.) online mixing set-up used.

3.3 Results and Discussion

3.3.1 Attempt to Online Detect Ni(III)/Reductive Elimination Product by MS

First, it was attempted to detect a potential Ni(III) intermediate (Scheme 3-1, species **7**) which is hypothesized to be generated prior to the reductive elimination taking place. To accomplish this, a modified reaction was performed (Scheme 3-3), wherein a nickel complex with 4,4'-di-tert-butyl-2,2'-bipyridine (dtbbpy) and 2,4-bis(trifluoromethyl)phenyl ligands (Scheme 3-3, species **1**) which was previously prepared was reacted in equal amounts with pyrrolidine and quinuclidine, to replace the chloride ligand with pyrrolidine (Scheme 3-3, species **2**). Catalytic amounts of iridium photocatalyst (((Ir[dF(CF_3)ppy]$_2$(dtbpy))PF_6) (Scheme 3-1, species **1**) were then added, and the mixture was tested by nESI-MS. The proposed structure of the reductive elimination product is shown in Scheme 3-3 as species **3**.

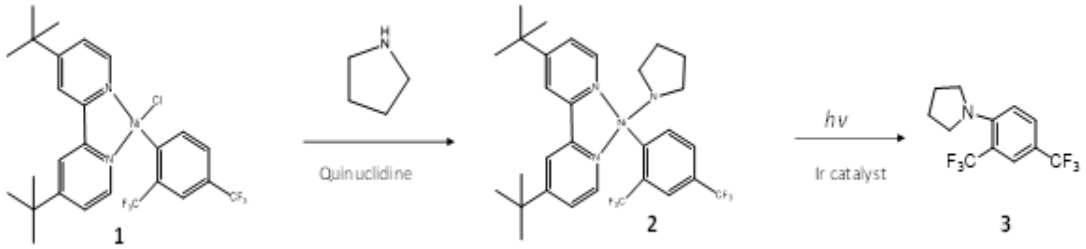

Scheme 3-3: Proposed reaction pathway studied using nESI/ESSI-MS.

To test this reaction, nESI-MS was used. A representative spectrum is shown in Figure 3-1. The spectra clearly showed the formation of a peak at *m/z* 651.24, corresponding to the replacement of the initial chloride ligand with pyrrolidine (Figure 3-2A), both with and without the coordination of ACN. It was proposed that this peak should be sensitive to the presence of irradiation and should exhibit a sharp decrease in peak intensity when the sample undergoes irradiation, to be replaced by a peak corresponding to a Ni(III) species, likely due to the loss of an electron from the species (Figure 3-2B). Indeed, when the laser was turned on, a sharp decrease in this peak intensity was observed, leading to an approximate 100x decrease in peak intensity. This result proved repeatable, as the peak would re-appear when the laser was turned off and could consistently be decreased by turning the laser back on (Figure 3-2C).

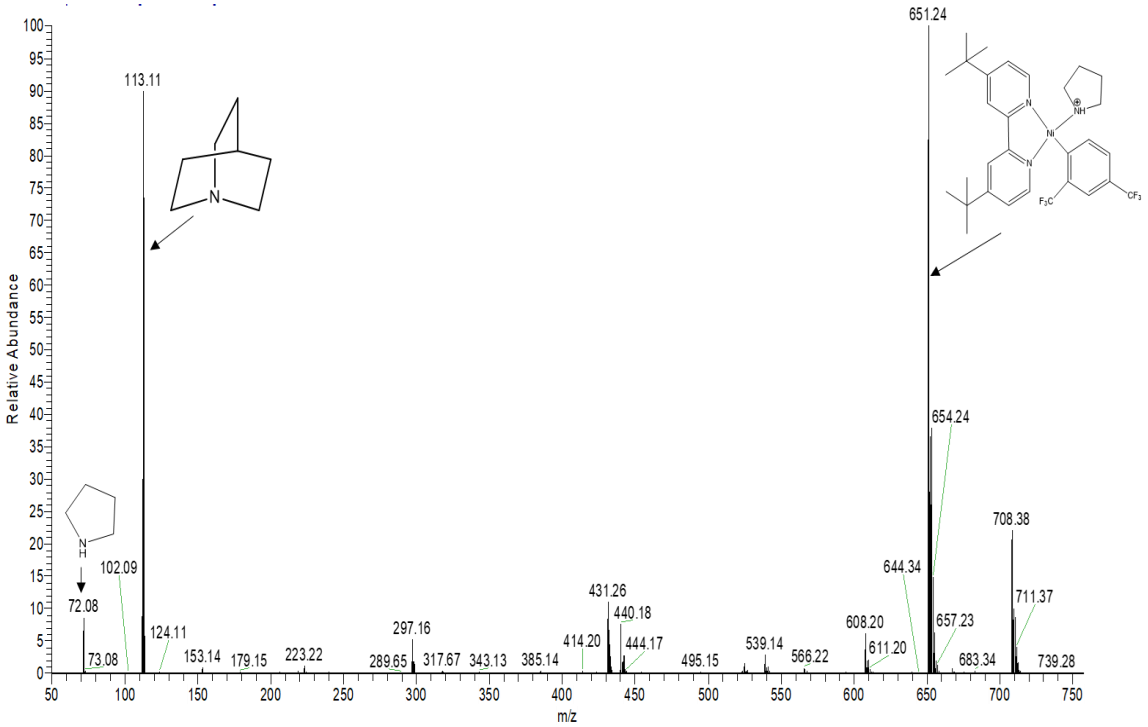

Figure 3-1: Representative MS spectrum for the mixture of nickel complex (Scheme 3-3, species **1**), pyrrolidine, quinuclidine and iridium photocatalyst following irradiation.

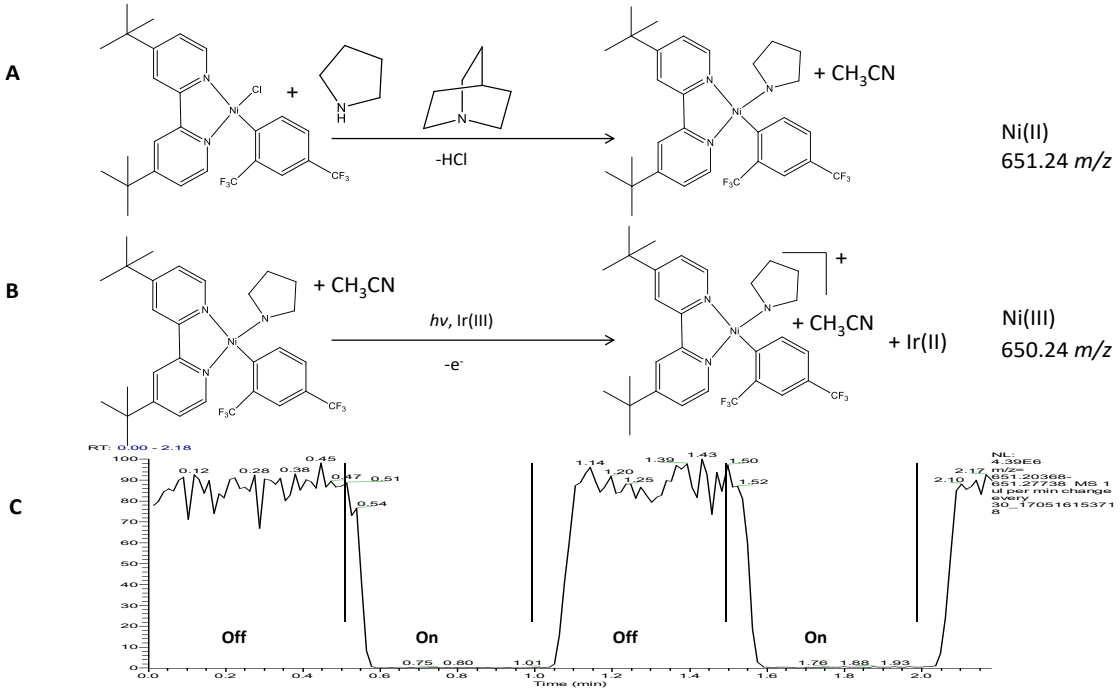

Figure 3-2: A.) Proposed reaction for the substitution of the chloride ligand on the starting nickel species with pyrrolidine. B.) Proposed reaction for the formation of Ni(III) species from the Ni(II) species previously formed. C.) Extracted ion current (EIC) of peak at *m/z* 651.24, demonstrating the large swings in peak intensity as the laser is switched on and off. The bars indicate the point in time where the laser was switched between on and off.

Unfortunately, the Ni(III) peak was not readily visible. Despite varying the flow rate and the technique used to ionize the solution, the proposed peak at *m/z* 650.24 was never observed with the desired intensity. While such a peak was observed on a few occasions, it was always low intensity and did not match up with the laser status as well as was desired (Figure 3-3). It is possible that the reason this peak could sometimes be observed would be due to the possibility of in-source oxidation from the ionization process. The reason that the peak seems to exhibit the opposite pattern, in that it is mainly present when the laser was turned off, maybe because the in-source oxidation would be much less likely to take place if the amount of *m/z* 651.24 decreases, which would match

the trend shown in Fig. 3-2C. In addition, the final product of the reaction was not observed.

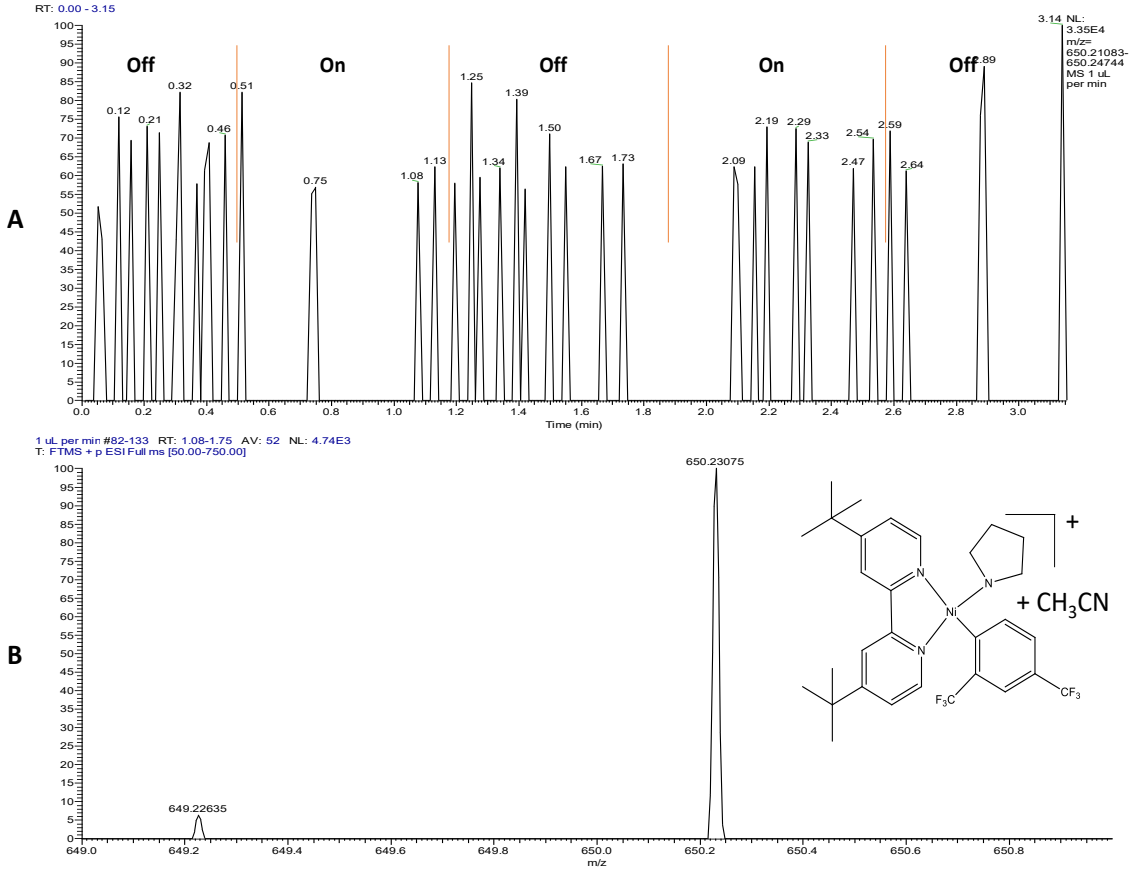

Figure 3-3: A.) EIC of peak at *m/z* 650.23, believed to potentially correspond to the Ni(III) species generated by the loss of an electron from 2. The laser status was initially set to off, and it was cycled between on and off every 30 seconds. B.) Zoomed-in spectrum showing peak at *m/z* 650.23 (theoretical mass: *m/z* 650.23487, mass error: 6.3 ppm)

3.3.2 Online Dehydrogenation of Pyrrolidine

While performing the aforementioned experiment, one feature noticed was the fluctuation of pyrrolidine peak intensity (*m/z* 72.08) with laser status. To investigate this, catalytic amounts of iridium photocatalyst was added to a sample solely containing

pyrrolidine (250 µM), and it was tested by both ESI and nESI-MS. It was found that the peak corresponding to pyrrolidine at *m/z* 72.08 (theoretical mass: *m/z* would exhibit a decrease when the laser was turned on (Figure 3-4A), while another peak at *m/z* 70.06 would greatly increase in intensity, believed to correspond to dihydropyrrole (Figure 3-4B).

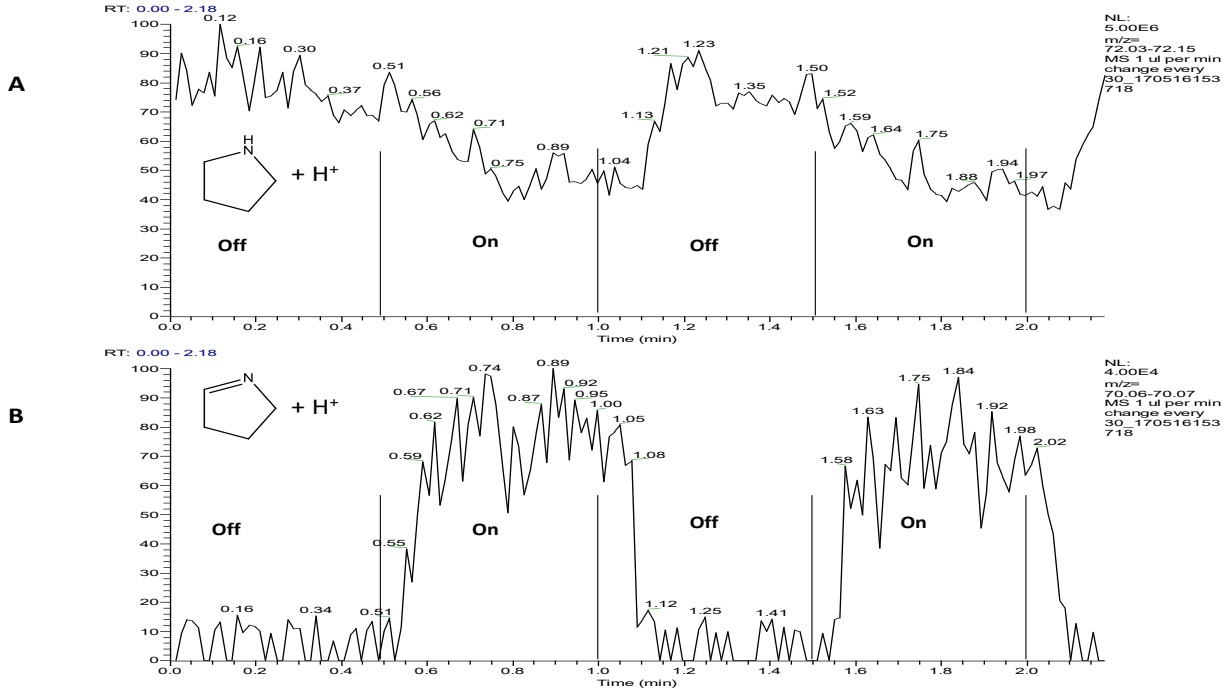

Figure 3-4: A.) EIC of *m/z* 72.08, corresponding to the protonated pyrrolidine. As the laser is cycled between off and on every 30 seconds, a decrease in peak intensity is observed. B.) EIC of *m/z* 70.06, believed to correspond to the protonated dihydropyrrole. When the laser is turned on, a large spike in peak intensity is observed, which then reverts to the smaller baseline level as soon as the laser is turned off.

To further test this, another experiment was performed where the nano-ESI flow of the sample was suspended and the tip of the capillary (serving as the irradiation window) was irradiated for 5 min (Figure 3-5). As expected, the spectrum obtained after the flow was resumed showed a much higher intensity of dihydropyrrole (theoretical

mass: *m/z* 70.06567, mass error: 4.70 ppm) relative to that before irradiation, while pyrrolidine (theoretical mass: *m/z* 72.08132, mass error: 4.02 ppm) showed a corresponding decrease in intensity.

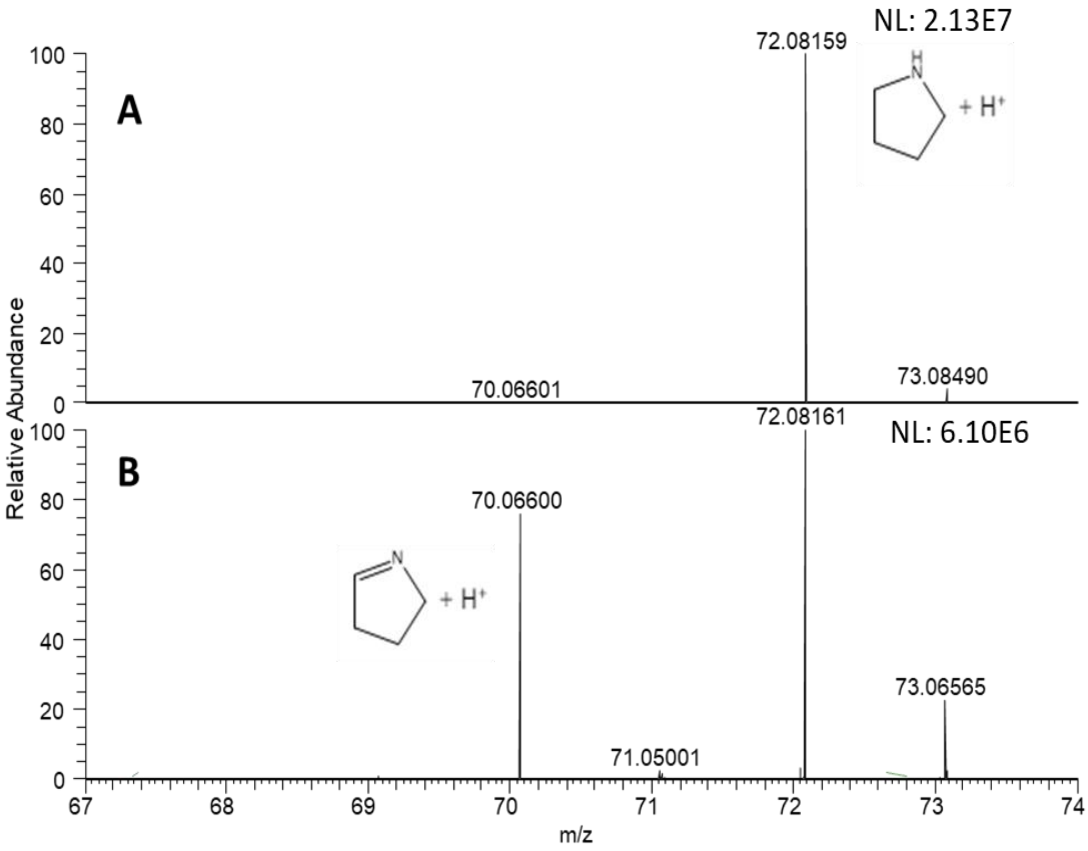

Figure 3-5: Mass spectra of pyrrolidine sample A.) without irradiation B.) following 5 minutes of irradiation in capillary tip

This may indicate that the iridium catalyst is able to interact with pyrrolidine, causing dehydrogenation to take place (Scheme 3-4A). It has previously been reported that other secondary amines, such as tetrahydroquinolines, can undergo dehydrogenation in the presence of light and an active photocatalyst.[30] However, in that work, the amines

used were part of aromatic systems, and a ruthenium-based photocatalyst was used (Scheme 3-4B), unlike the photocatalyst used here.

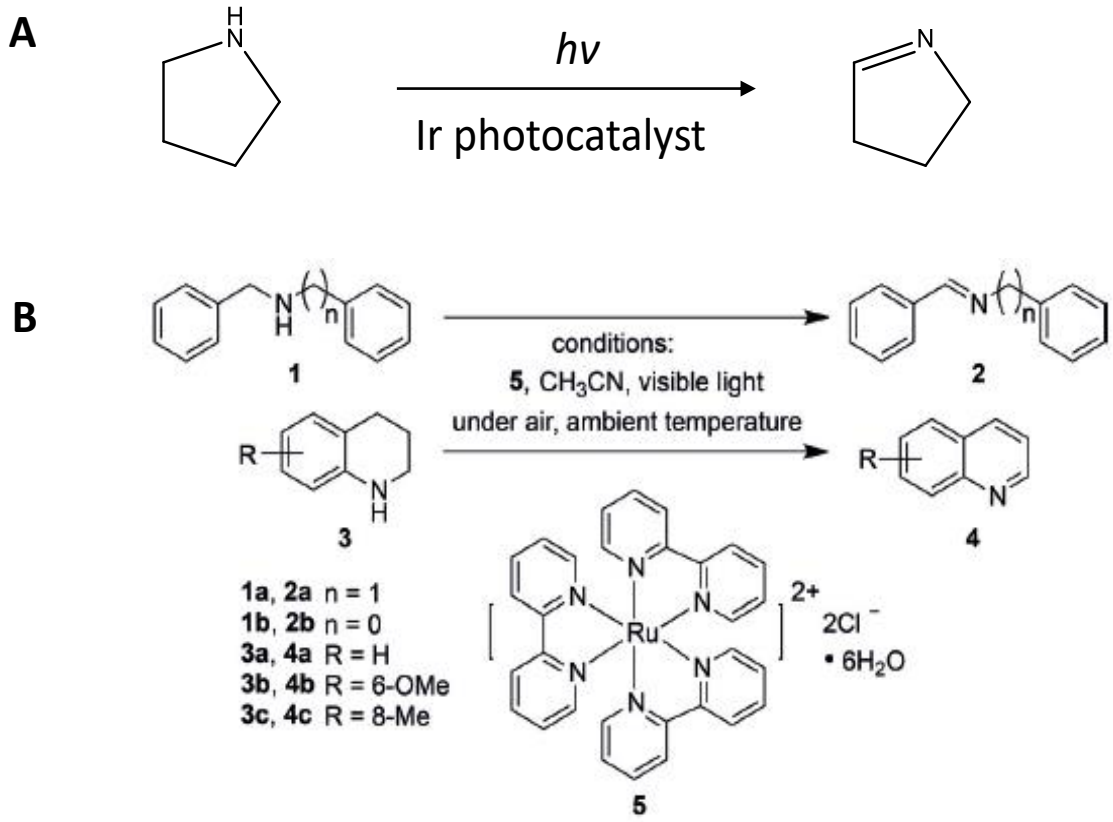

Scheme 3-4: A.) Reaction studied in this work of the dehydrogenation of pyrrolidine using an iridium photocatalyst. B.) Reaction previously studied in literature of tetrahydroquinolines using a ruthenium-based catalyst[30].

To investigate the viability of this reaction on a larger scale as well as the ability of sunlight to drive the reaction, another experiment was devised. A pyrrolidine analog, 2-methylpyrrolidine (Scheme 3-5, 100 mM) was mixed with iridium photocatalyst (700 μM) and irradiated in a window sill for 48 hours. After irradiation, the sample was diluted to 10 μM, and was analyzed by MS using nano-ESI (Figure 3-6C). In addition, two controls were created, one where the sample did not include iridium but was still in

the window (Figure 3-6A), and another where the sample did contain iridium (Figure 3-6B), but the sample was covered with foil to prevent sunlight from reaching it. To allow comparison between spectra, pyrrolidine was also added into the sample prior to injection into the MS to act as an internal standard, due to its similar ionization efficiency. It was observed that the sample with iridium and exposed to sunlight exhibited the same potential dehydrogenation reaction as pyrrolidine was shown to, demonstrating the appearance of a peak at *m/z* 84.08, believed to correspond to the 2-methyldihydropyrrole, and a decrease in the peak at *m/z* 86.10, corresponding to 2-methylpyrrolidine. This intensity change was not 1:1, which may indicate the presence of side reactions also occurring, however.

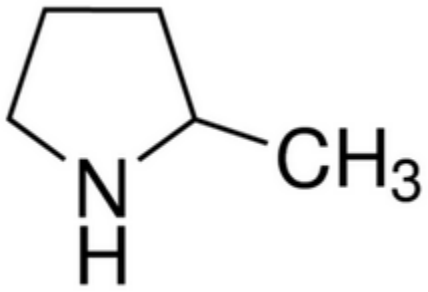

Scheme 3-5: 2-methylpyrrolidine

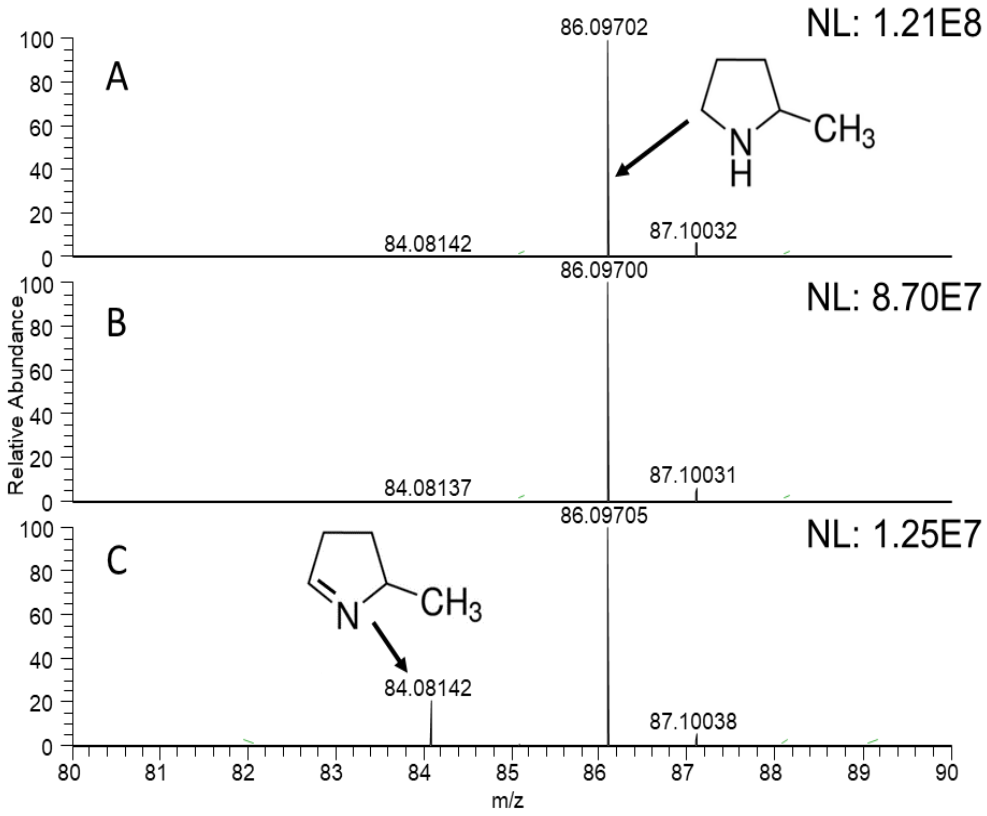

Figure 3-6: Mass spectra showing the region of 2-methylpyrrolidine and its dehydrogenated form after 48 hours when A.) sample is irradiated without iridium photocatalyst; B.) sample is not irradiated but includes iridium photocatalyst and C.) sample both includes iridium and was irradiated.

3.3.3 Monitoring of Online Mixed Solution Upon Irradiation

One potential reason for the issues in detecting product was that the to inject the sample into the MS, the reaction conditions must be changed from those initially reported. To circumvent this, the online mixing set-up shown above was used. Due to the much weaker ionization efficiency, it allows for higher concentrations to be used for mixing, followed by direct ionization. $NiCl_2$-ethylene glycol dimethyl ether (Scheme 3-6, species **4**) was used as the starting nickel species, and then reacted with the dtbbpy ligand. The resulting mixture (Scheme 3-5, species **5**) was then added to a vial containing

1,4-diazobicyclo[2.2.2]octane (DABCO), pyrrolidine, and 4-bromoacetophenone, loosely following the procedure stated in Corcoran[1g], to generate product (Scheme 3B, 6).

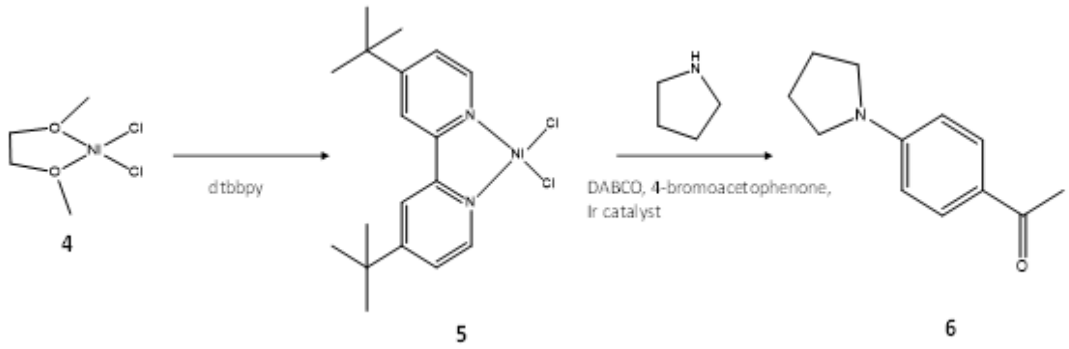

Scheme 3-6: Reaction pathway used for online mixing experiment

This mixture was placed on a blue LED providing irradiation and was sampled as previously described every 10 min by switching the gas flow through the ionization source on. It was observed that the final product of this reaction could be observed, as well as a few other peaks signifying modifications to the product, likely due to reactions taking place between the product and left-over pyrrolidine or DABCO (Figure 3-7). This indicates that significant side reactions may happen during this reaction, particularly in the gas-phase conditions the sample undergoes during MS and may explain the difficulty in observing product for the online reaction despite the presence of what should be its precursor.

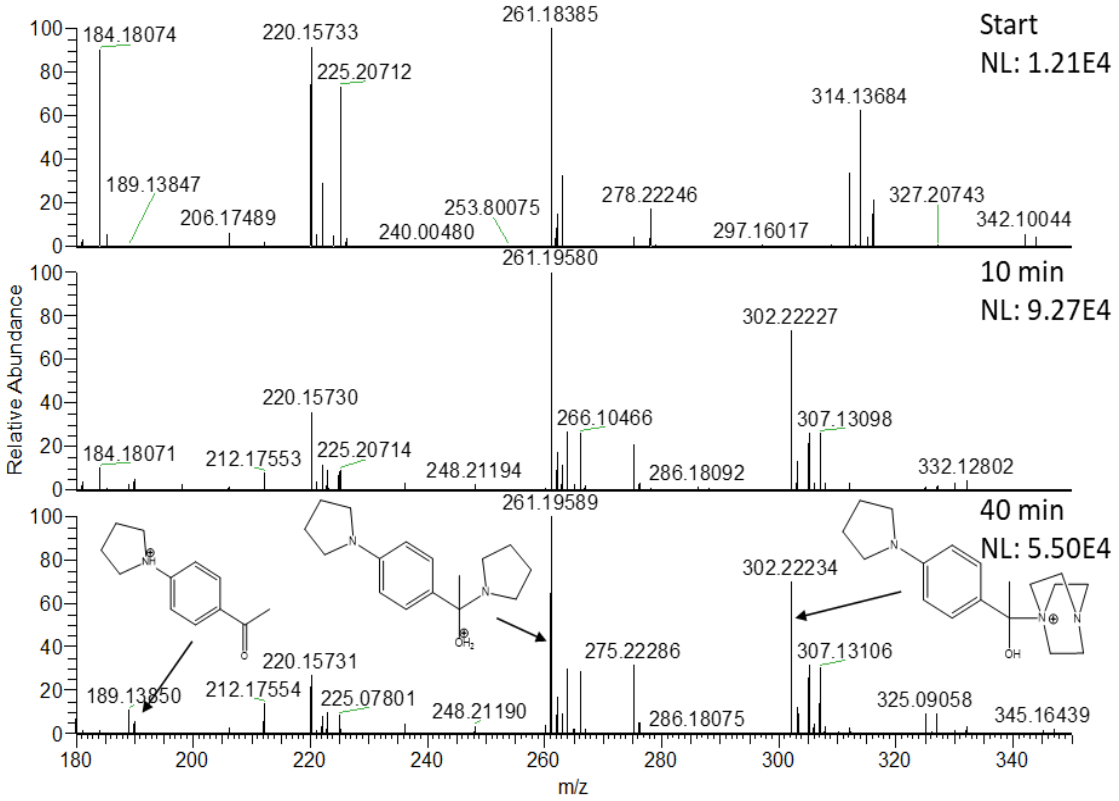

Figure 3-7: Mass spectra showing the region in which product, as well as product derivatives, formed during the online reaction at times of 0 min, 10 min, and 40 min. Three main forms of product were formed, the first being the intended at *m/z* 190.12 (theoretical mass: *m/z* 190.12264, mass error: 1.0 ppm), the second being product which has further reacted with pyrrolidine at *m/z* 261.20 (theoretical mass: *m/z* 261.19614, mass error: 1.0 ppm), and the third being product reacted with DABCO at *m/z* 302.22 (theoretical mass: *m/z* 302.22269, mass error: 1.2 ppm).

3.4 Conclusions

In conclusion, while Ni(III) was not able to be observed with any certainty, the ability of mass spectrometry to monitor online photochemical reactions was shown. In addition, a potentially beneficial side reaction involving the dehydrogenation of pyrrolidine was observed and reported for the first time, which could offer an improvement over currently used methods. Using online mixing and reaction monitoring,

it was also possible to identify the product of the reaction, as well as potential products from side reactions.

CHAPTER 4: SUMMARY AND FUTURE WORK

In summary, this thesis demonstrates the ability of mass spectrometry to be coupled with both electrochemistry and photochemistry for capturing reaction intermediates and elucidating reaction mechanisms. Future work with carbazole and triphenylamine includes using online DESI-MS to get potentially more reliable data and testing other methods/compounds to see if the same proposed reaction mechanism is observed. In addition, to determine the kinetics of the TPA reaction, such as the rate of charge transfer to see how favorable it is. For the nickel reductive elimination, future work includes trying different ligand combinations to determine if they may generate a longer-lived Ni(III) species, which may be easier to observe with MS. For the dehydrogenation experiments, future work includes using nuclear magnetic resonance spectroscopy to get a better idea of the yield of the product, as well as determining the true location of the proposed double found formed.

REFERENCES

(1) Kicman, A. T.; Parkin, M. C.; Iles, R. K. An Introduction to Mass Spectrometry Based Proteomics—Detection and Characterization of Gonadotropins and Related Molecules. *Molecular and Cellular Endocrinology* **2007**, *260–262*, 212–227. https://doi.org/10.1016/j.mce.2006.02.022.

(2) McLafferty, F. W. A Century of Progress in Molecular Mass Spectrometry. *Annual Review of Analytical Chemistry* **2011**, *4* (1), 1–22. https://doi.org/10.1146/annurev-anchem-061010-114018.

(3) Kandiah, M.; Urban, P. L. Advances in Ultrasensitive Mass Spectrometry of Organic Molecules. *Chem Soc Rev* **2013**, *42* (12), 5299–5322. https://doi.org/10.1039/c3cs35389c.

(4) Tsednee, M.; Huang, Y.-C.; Chen, Y.-R.; Yeh, K.-C. Identification of Metal Species by ESI-MS/MS through Release of Free Metals from the Corresponding Metal-Ligand Complexes. *Scientific Reports* **2016**, *6*, 26785. https://doi.org/10.1038/srep26785.

(5) Siuzdak, G. An Introduction to Mass Spectrometry Ionization: An Excerpt from The Expanding Role of Mass Spectrometry in Biotechnology, 2nd Ed.; MCC Press: San Diego, 2005. *JALA: Journal of the Association for Laboratory Automation* **2004**, *9* (2), 50–63. https://doi.org/10.1016/j.jala.2004.01.004.

(6) Foltz, R. L. Recent Applications of Mass Spectrometry in Forensic Toxicology. *International Journal of Mass Spectrometry and Ion Processes* **1992**, *118–119*, 237–263. https://doi.org/10.1016/0168-1176(92)85064-7.

(7) Deng, G.; Sanyal, G. Applications of Mass Spectrometry in Early Stages of Target Based Drug Discovery. *Journal of Pharmaceutical and Biomedical Analysis* **2006**, *40* (3), 528–538. https://doi.org/10.1016/j.jpba.2005.08.038.

(8) Medved, M. Mass Spectrometry in Environmental Analysis. *Rapid Communications in Mass Spectrometry* **1991**, *5* (1), 11–14. https://doi.org/10.1002/rcm.1290050104.

(9) Lu, Y.; Chen, W. Application of Mass Spectrometry in the Synthesis and Characterization of Metal Nanoclusters. *Anal. Chem.* **2015**, *87* (21), 10659–10667. https://doi.org/10.1021/acs.analchem.5b00848.

(10) Cappiello, A.; Famiglini, G.; Mangani, F.; Palma, P. New Trends in the Application of Electron Ionization to Liquid Chromatography-Mass Spectrometry Interfacing. *Mass Spectrom Rev* **2001**, *20* (2), 88–104. https://doi.org/10.1002/mas.1004.

(11) Munson, M. S. B.; Field, F. H. Chemical Ionization Mass Spectrometry. I. General Introduction. *Journal of the American Chemical Society* **1966**, *88* (12), 2621–2630. https://doi.org/10.1021/ja00964a001.

(12) Ho, C.; Lam, C.; Chan, M.; Cheung, R.; Law, L.; Lit, L.; Ng, K.; Suen, M.; Tai, H. Electrospray Ionisation Mass Spectrometry: Principles and Clinical Applications. *Clin Biochem Rev* **2003**, *24* (1), 3–12.

(13) Wilm, M. Principles of Electrospray Ionization. *Mol Cell Proteomics* **2011**, *10* (7). https://doi.org/10.1074/mcp.M111.009407.

(14) Van Berkel, G. J.; Kertesz, V.; Ford, M. J.; Granger, M. C. Efficient Analyte Oxidation in an Electrospray Ion Source Using a Porous Flow-through Electrode Emitter. *Journal of the American Society for Mass Spectrometry* **2004**, *15* (12), 1755–1766. https://doi.org/10.1016/j.jasms.2004.08.013.

(15) Takáts, Z.; Wiseman, J. M.; Cooks, R. G. Ambient Mass Spectrometry Using Desorption Electrospray Ionization (DESI): Instrumentation, Mechanisms and Applications in Forensics, Chemistry, and Biology. *Journal of Mass Spectrometry* **2005**, *40* (10), 1261–1275. https://doi.org/10.1002/jms.922.

(16) Takáts, Z.; Wiseman, J. M.; Gologan, B.; Cooks, R. G. *Science* **2004**, *306*, 471.

(17) Haag, A. M. Mass Analyzers and Mass Spectrometers. In *Modern Proteomics – Sample Preparation, Analysis and Practical Applications*; Mirzaei, H., Carrasco, M., Eds.; Advances in Experimental Medicine and Biology; Springer International Publishing: Cham, 2016; pp 157–169. https://doi.org/10.1007/978-3-319-41448-5_7.

(18) March, R. E. An Introduction to Quadrupole Ion Trap Mass Spectrometry. *Journal of Mass Spectrometry* **1997**, *32* (4), 351–369. https://doi.org/10.1002/(SICI)1096-9888(199704)32:4<351::AID-JMS512>3.0.CO;2-Y.

(19) Zubarev, R. A.; Makarov, A. Orbitrap Mass Spectrometry. *Analytical Chemistry* **2013**, *85* (11), 5288–5296. https://doi.org/10.1021/ac4001223.

(20) Koppenaal, D. W.; Barinaga, C. J.; Denton, M. B.; Sperline, R. P.; Hieftje, G. M.; Schilling, G. D.; Andrade, F. J.; Barnes, J. H. Just as Laser Eye Surgery Has Restored Fading Human Vision, New Technologies Are Needed to Improve Ion "Chemical Vision" Detection. 10.

(21) Hendel, S. J.; Young, E. R. Introduction to Electrochemistry and the Use of Electrochemistry to Synthesize and Evaluate Catalysts for Water Oxidation and

Reduction. *Journal of Chemical Education* **2016**, *93* (11), 1951–1956. https://doi.org/10.1021/acs.jchemed.6b00230.

(22) Portychová, L.; Schug, K. A. Instrumentation and Applications of Electrochemistry Coupled to Mass Spectrometry for Studying Xenobiotic Metabolism: A Review. *Analytica Chimica Acta* **2017**, *993*, 1–21. https://doi.org/10.1016/j.aca.2017.08.050.

(23) Faber, H.; Vogel, M.; Karst, U. Electrochemistry/Mass Spectrometry as a Tool in Metabolism Studies—A Review. *Analytica Chimica Acta* **2014**, *834*, 9–21. https://doi.org/10.1016/j.aca.2014.05.017.

(24) Sánchez-Ortega, A.; Sampedro, M. C.; Unceta, N.; Goicolea, M. A.; Barrio, R. J. Solid-Phase Microextraction Coupled with High Performance Liquid Chromatography Using on-Line Diode-Array and Electrochemical Detection for the Determination of Fenitrothion and Its Main Metabolites in Environmental Water Samples. *Journal of Chromatography A* **2005**, *1094* (1), 70–76. https://doi.org/10.1016/j.chroma.2005.07.089.

(25) Jahn, S.; Karst, U. Electrochemistry Coupled to (Liquid Chromatography/) Mass Spectrometry—Current State and Future Perspectives. *Journal of Chromatography A* **2012**, *1259*, 16–49. https://doi.org/10.1016/j.chroma.2012.05.066.

(26) Scholz, R.; Palatzky, P.; Matysik, F.-M. Simulation of Oxidative Stress of Guanosine and 8-Oxo-7,8-Dihydroguanosine by Electrochemically Assisted Injection–Capillary Electrophoresis–Mass Spectrometry. *Anal Bioanal Chem* **2014**, *406* (3), 687–694. https://doi.org/10.1007/s00216-013-7500-2.

(27) Ramamurthy, V.; Turro, N. J. Photochemistry: Introduction. *Chem. Rev.* **1993**, *93* (2), 585–586. https://doi.org/10.1021/cr00018a600.

(28) Brummel, O.; Waidhas, F.; Bauer, U.; Wu, Y.; Bochmann, S.; Steinrück, H.-P.; Papp, C.; Bachmann, J.; Libuda, J. Photochemical Energy Storage and Electrochemically Triggered Energy Release in the Norbornadiene–Quadricyclane System: UV Photochemistry and IR Spectroelectrochemistry in a Combined Experiment. *The Journal of Physical Chemistry Letters* **2017**, *8* (13), 2819–2825. https://doi.org/10.1021/acs.jpclett.7b00995.

(29) Chatani, S.; J. Kloxin, C.; N. Bowman, C. The Power of Light in Polymer Science: Photochemical Processes to Manipulate Polymer Formation, Structure, and Properties. *Polymer Chemistry* **2014**, *5* (7), 2187–2201. https://doi.org/10.1039/C3PY01334K.

(30) Chen, S.; Wan, Q.; Badu-Tawiah, A. K. Picomole-Scale Real-Time Photoreaction Screening: Discovery of the Visible-Light-Promoted Dehydrogenation of Tetrahydroquinolines under Ambient Conditions. *Angewandte Chemie International Edition* **2016**, *55* (32), 9345–9349. https://doi.org/10.1002/anie.201603530.

(31) Keizer, S. P.; Han, W.; Stillman, M. J. Photochemically-Induced Radical Reactions of Zinc Phthalocyanine. *Inorganic Chemistry* **2002**, *41* (2), 353–358. https://doi.org/10.1021/ic010688w.

(32) Ma, X.; Zhao, X.; Li, J.; Zhang, W.; Cheng, J.-X.; Ouyang, Z.; Xia, Y. Photochemical Tagging for Rapid Quantitation of Unsaturated Fatty Acids by Mass Spectrometry. *Anal Chem* **2016**, *88* (18), 8931–8935. https://doi.org/10.1021/acs.analchem.6b02834.

(33) Grazulevicius, J. V.; Strohriegl, P.; Pielichowski, J.; Pielichowski, K. Carbazole-Containing Polymers: Synthesis, Properties and Applications. *Progress in Polymer Science* **2003**, *28* (9), 1297–1353. https://doi.org/10.1016/S0079-6700(03)00036-4.

(34) Organic Dyes Containing Carbazole as Donor and π-Linker: Optical, Electrochemical, and Photovoltaic Properties - ACS Applied Materials & Interfaces (ACS Publications) https://pubs-acs-org.proxy.library.ohio.edu/doi/10.1021/am404948w

(35) Karon, K.; Lapkowski, M. Carbazole Electrochemistry: A Short Review. *J Solid State Electrochem* **2015**, *19* (9), 2601–2610. https://doi.org/10.1007/s10008-015-2973-x.

(36) Ambrose, J. F.; Nelson, R. F. Anodic Oxidation Pathways of Carbazoles. *Journal of The Electrochemical Society* **1968**, *115* (11), 1159. https://doi.org/10.1149/1.2410929.

(37) Ambrose, J. F.; Carpenter, L. L.; Nelson, R. F. Electrochemical and Spectroscopic Properties of Cation Radicals III . Reaction Pathways of Carbazolium Radical Ions. *J. Electrochem. Soc.* **1975**, *122* (7), 876–894. https://doi.org/10.1149/1.2134365.

(38) Liu, Y.-M.; Perry, R. H. Paper-Based Electrochemical Cell Coupled to Mass Spectrometry. *Journal of The American Society for Mass Spectrometry* **2015**, *26* (10), 1702–1712. https://doi.org/10.1007/s13361-015-1224-9.

(39) Liu, Y.-M.; G. Nicolau, B.; Esbenshade, J. L.; Gewirth, A. A. Characterization of the Cathode Electrolyte Interface in Lithium Ion Batteries by Desorption Electrospray Ionization Mass Spectrometry. *Anal. Chem.* **2016**, *88* (14), 7171–7177. https://doi.org/10.1021/acs.analchem.6b01292.

(40) Qiu, R.; Zhang, X.; Luo, H.; Shao, Y. Mass Spectrometric Snapshots for Electrochemical Reactions. *Chem. Sci.* **2016**, *7* (11), 6684–6688. https://doi.org/10.1039/C6SC01978A.

(41) Brown, T. A.; Chen, H.; Zare, R. N. Identification of Fleeting Electrochemical Reaction Intermediates Using Desorption Electrospray Ionization Mass Spectrometry. *J. Am. Chem. Soc.* **2015**, *137* (23), 7274–7277. https://doi.org/10.1021/jacs.5b03862.

(42) Cheng, H.; Yan, X.; Zare, R. N. Two New Devices for Identifying Electrochemical Reaction Intermediates with Desorption Electrospray Ionization Mass Spectrometry. *Anal. Chem.* **2017**, *89* (5), 3191–3198. https://doi.org/10.1021/acs.analchem.6b05124.

(43) Liu, C, Hivick, B. E., Pan, Y., Chen H. *Manuscript in preparation*

(44) Ledwith, A.; Sambhi, M. Electron-Transfer Reactions with the Tropylium Cation. *Chem. Commun. (London)* **1965**, No. 4, 64–65. https://doi.org/10.1039/C19650000064.

(45) Iles, D. H.; Ledwith, A. Acid-Catalysed Electron-Transfer Reactions of Lead Tetra-Acetate: Stable Cation-Radicals from Carbazole Derivatives. *Chem. Commun. (London)* **1968**, No. 9, 498–499. https://doi.org/10.1039/C19680000498.

(46) Goto, M.; Park, H.; Otsuka, K.; Oyama, M. Kinetics of the Decay Reactions of the N,N-Dimethyl-p-Toluidine Cation Radical in Acetonitrile. Acid−Base Interaction to Promote the CH2−CH2 Bonding. *J. Phys. Chem. A* **2002**, *106* (35), 8103–8108. https://doi.org/10.1021/jp026073h.

(47) Pragst, F.; Niazymbetov, M. Electrogenerated Chemiluminescence in Mechanistic Investigations of Electroorganic Reactions: Part VI. Sensitive Detection of Cation Radicals by Bis-[1,2,3-Trimethyl-2,3-Dihydrobenzimidazolyl-(2)]/Luminophor Systems. *Journal of Electroanalytical Chemistry and Interfacial Electrochemistry* **1986**, *197* (1), 245–264. https://doi.org/10.1016/0022-0728(86)80153-X.

(48) Zivolic, F.; Zancanaro, F.; Favretto, D.; Ferrara, S. D.; Seraglia, R.; Traldi, P. Pneumatically Assisted Desorption/Ionization: 1. Some Thoughts on the Possible Ionization Mechanism(S). *J Mass Spectrom* **2010**, *45* (4), 411–420. https://doi.org/10.1002/jms.1727.

(49) Cai, Y., Wang, J., Zhang, Y., Li, Z., Hu, D., Zheng, N., Chen, H. *J. Am. Chem. Soc*., 2017, **139**, 12259-12266.

(50) Mahmood, A. Triphenylamine Based Dyes for Dye Sensitized Solar Cells: A Review. *Solar Energy* **2016**, *123*, 127–144. https://doi.org/10.1016/j.solener.2015.11.015.

(51) Song, Y.; Di, C.; Yang, X.; Li, S.; Xu, W.; Liu, Y.; Yang, L.; Shuai, Z.; Zhang, D.; Zhu, D. A Cyclic Triphenylamine Dimer for Organic Field-Effect Transistors with High Performance. *J. Am. Chem. Soc.* **2006**, *128* (50), 15940–15941. https://doi.org/10.1021/ja064726s.

(52) Manifar, T.; Rohani, S. Synthesis and Analysis of Triphenylamine: A Review. *The Canadian Journal of Chemical Engineering* **2008**, *82* (2), 323–334. https://doi.org/10.1002/cjce.5450820213.

(53) Oyama, M.; Nozaki, K.; Okazaki, S. Pulse-Electrolysis Stopped-Flow Method for the Electrospectroscopic Analysis of Short-Lived Intermediates Generated in the Electrooxidation of Triphenylamine. *Anal. Chem.* **1991**, *63* (14), 1387–1392. https://doi.org/10.1021/ac00014a010.

(54) (a) Prier, C. K.; Rankic, D. A.; MacMillan, D. W. C. Chem. Rev. 2013, 113, 5322-5363. (b) Xuan, J.; Xiao, W.-J. Angew. Chem., Int. Ed. 2012, 51, 6828-6838. (c) Fukuzumi, S.; Ohkubo, K. Chem. Sci. 2013, 4, 561-574. (d) Yoon, T. P. ACS. Catal. 2013, 3, 895-902. (e) Romero, N. A.; Nicewicz, D. A. Chem. Rev. 2016, DOI: 10.1021/acs.chemrev.6b00057. f) Kainz, Q. M.; Matier, C. D.; Bartoszewicz, A.; Zultanski, S. L.; Peters, J. C.; Fu, G. C. Science 2016, 351, 681-684. (g) Corcoran, E. B.; Pirnot, M. T.; Lin, S.; Dreher, D. A.; DiRocco, D. A.; Davies, I. A.; Buchwald, S. L.; MacMillan, D. W. C. Science 2016, 353, 279-283

(55) Terrett, J. A.; Cuthbertson, J. D.; Shurtleff, V. W.; MacMillan, D. W. C. Nature 2015, 524, 330–334.

(56) Ram; Kaur1, E.; Rani1, V.; Abbot1, V.; Kapoor2, Y.; Konar3, D.; Kumar1, K.; 2; 3. Recent Synthetic and Medicinal Perspectives of Pyrroles: An Overview. *Journal of Pharmaceutical Chemistry & Chemical Science* **2017**, *1* (1).

(57) Huang, H.; Tang, L.; Cai, J.; Deng, G.-J. Mild and Ambient Annulations for Pyrrole Synthesis from Amines and Arylacetaldehydes. *RSC Adv.* **2016**, *6* (9), 7011–7014. https://doi.org/10.1039/C5RA24006A.

(58) Kayser, L. V.; Vollmer, M.; Welnhofer, M.; Krikcziokat, H.; Meerholz, K.; Arndtsen, B. A. Metal-Free, Multicomponent Synthesis of Pyrrole-Based π-Conjugated Polymers from Imines, Acid Chlorides, and Alkynes. *J. Am. Chem. Soc.* **2016**, *138* (33), 10516–10521. https://doi.org/10.1021/jacs.6b05035.

(59) Farahi, M. A New Protocol for One-Pot Synthesis of Tetrasubstituted Pyrroles Using Tungstate Sulfuric Acid as a Reusable Solid Catalyst. *Tetrahedron letters* **2016**, *v. 57*, 1582–1584. https://doi.org/10.1016/j.tetlet.2016.02.101.

Thesis and Dissertation Services